CRITICAL ANALYSIS OF AN ELECTRO-HYDRAULIC SERVO VALVE OPENING UNDER STEADY-STATE AND TRANSIENT CONDITIONS

A Thesis By

Charles Porter

Presented to the Jackson College of Graduate Studies for the University of Central Oklahoma in Partial Fulfillment of the Requirements for the Degree of

MASTER OF SCIENCE IN ENGINEERING PHYSICS – MECHANICAL ENGINEERING

JULY 2020

CRITICAL ANALYSIS OF AN ELECTRO-HYDRAULIC SERVO VALVE OPENING UNDER
STEADY-STATE AND TRANSIENT CONDITIONS

Thesis Title

Charles Porter

Author's Name

7/27/2020

Date

Jackson College of Graduate Studies at the University of Central Oklahoma

A THESIS APPROVED FOR

By

Evan Lemley   7/27/2020

Committee Chairperson

7/27/20

Committee Member

7/27/2020

Committee Member

Committee Member

Acknowledgments

Abstract

Electro-Hydraulic servo valves (EHSV) are used extensively in industrial applications due to their lightweight design, inexpensive manufacturing, simple operating technology, and modularity. EHSV are used in military, industrial, aviation, and other applications. The engineering design, testing and prototyping of EHSV as implemented in a given fluid system can be expensive and time consuming. Improvements made in computational modeling and simulation of system designs that include EHSV can reduce time and cost in implementing EHSV in fluid systems by leveraging computational capabilities to predict performance of EHSV.

The operating principles and flow effects of EHSV used in industry are often difficult to predict in a particular fluid system. Simulation of EHSV has the potential to improve prediction of performance in given systems, but the challenge is that simulating flow in EHSV can be very challenging due to transient (TR) flow and dynamic geometries.

This thesis focuses on simulating fluid flow at various times as an EHSV is opening to determine flow parameters for a specific industrial EHSV design utilizing steady-state (SS) and TR modeling. Consistency between SS and TR techniques is calculated. Data from a similar experimental system is compared to determine simulation accuracy and evaluate modeling effectiveness of SS and TR techniques.

The standard k-ε method for modeling turbulence in the system was utilized to simulate a valve opening under both SS and TR conditions. In the TR simulation dynamic meshing was utilized for the region where the mesh moves model valve opening.

Simulation results show similarities in flow profiles and parameters between SS and TR models. Dynamic meshing near the valve opening, when the valve just begins to open, induces error throughout the system and effects all flow field parameters studied in this thesis.

The SS and TR models each have an area where their accuracy is optimum. Steady-state modeling provides better accuracy where dynamic meshing may induce error for small geometries and gaps, while dynamic TR modeling is more accurate for larger less complicated mesh structures. The SS simulation averaged a 7.96% difference from the experimental values over the range of $1.95mm \geq X_L \geq 4.17mm$, where X_L is the distance a control spool has moved to open the valve, while the TR simulation averaged 7.81% difference. The difference in accuracy between the two different type of models would be negligible in most applications for valve design. The TR simulation averaged an 7.86% difference from the experimental values over the range of $4.17\ mm \geq X_L \geq 7.87\ mm$, while the SS simulation averaged 17.52% accuracy over that same range. A difference of approximately 9.66% may be significant enough to effect design.

These values provide insight into simplifying simulated models for applications where accuracy reduction is an acceptable trade-off for time and computational expense related to performing more complicated and difficult models such as a dynamic and transient model. Further research may be conducted into simplifying models and simulation for industry design applications.

Contents

Figures

Nomenclature

Symbol	Definition
X_L	Stroke
A	Work Port A
B	Work Port B
T	Tank or Reservoir Port
P	Pump or Pressure Port
∇	Gradient
ρ	Density
t	Time
V	Velocity Vector
g	Gravity
p	Pressure
τ	Shear Stress
x	Longitudinal Axis
y	Vertical Axis
z	Transverse Axis
u	x-Direction Velocity
v	y-Direction Velocity
w	z-Direction Velocity
μ	Dynamic Viscosity
k	TKE
ε	Dissapation Rate of TKE
P	Turbulent Production
D	Turbulent Destruction
L	Entrance Length
d	Diameter
Re	Reynolds Number
$C_{1\varepsilon}$ $C_{2\varepsilon}$ σ_ε C_μ σ_k	Standard k-ε Turbulence Empirical

Acronym	Definition
EHSV	Electrohydraulic Servo Valve
TR	Transient
SS	Steady-State
TKE	Turbulent Kinetic Energy

Chapter 1 Introduction

Valves are used in a wide variety of applications and are becoming increasingly more intelligent

and precise. Valves encompass any device used for stopping or controlling the flow of a liquid or

material and can be used as safety devices, control systems and much more. Many simple

hydraulic systems utilize a servo-type valve to enable an operator to have precise control over a

variety of parameters. A servo is a control system which measures its own output and forces the

output to quickly and accurately follow a command signal [1]. Servo-valves can be used to

control pressure, flow, or both. These typically have feedback controlling valve position from a

neutral position referred to as stroke.

1.1 Electro-Hydraulic Servo Valve Background

Servomechanisms can be classified as electro-pneumatic, electro-mechanical and electro-

hydraulic. Electro-hydraulic valves utilize electric current controlling flow of hydraulic oil,

Electro-pneumatic use air as the working fluid, and Electro-mechanical utilize a mechanical

mechanism. Depending on cost, performance, duty cycle and other design parameters, an

engineer must select the valve according to the application. Figure 1 shows performance ranges

for each of the valve types.
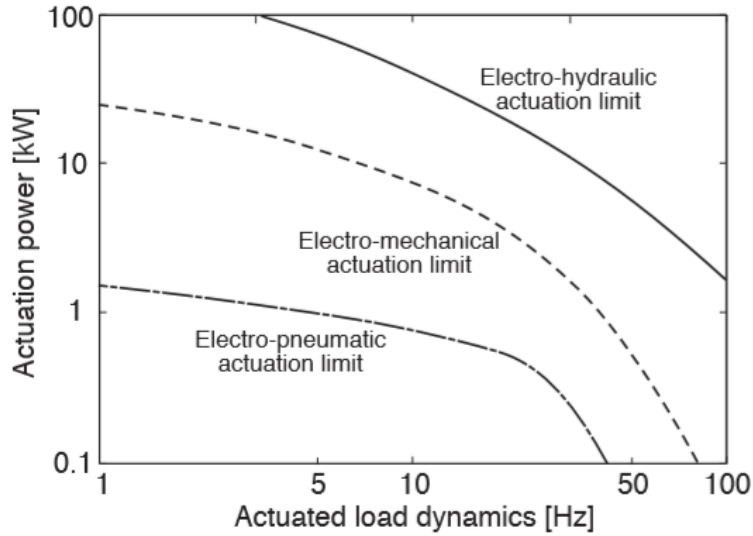
Figure 1.1: Servo valve performance characteristics [1]

Due to the simplicity, cost and performance characteristics, electro-hydraulic servo valves

(EHSV) have been developed to accomplish nearly every task [1]. EHSV can be further divided

into position, velocity, or force type valves. The most widely used valve is a sliding or linear

position valve that employs spool type construction [1]. These valves utilize an electrical output

indicating a position or stroke, which allows the valve to adjust its position based on a command

input. Figure 1.2 shows common configurations of these valves.
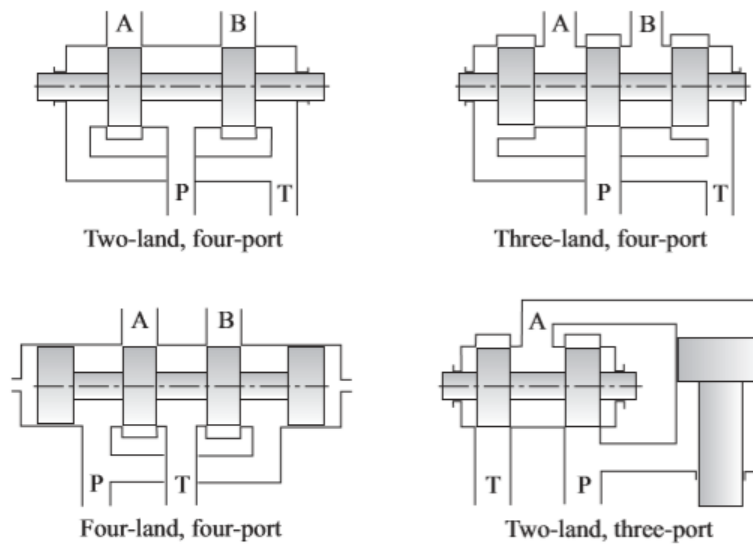
Figure 1.2: EHSV configuration

In Figure 1.2 A and B refer to the work ports to which fluid is directed to perform hydraulic work. The notation, P, indicates the incoming pressurized fluid, and T indicates the path the fluid travels to return to the tank or reservoir.

An important aspect of valve performance is related to the type of valve center, which may be closed center, critical center or open center as shown in Figure 1.1Figure 1.3. These configurations define the flow gain characteristics, which are shown in Figure 1.3 as a plot of flow rate vs valve stroke. Valve stroke is the distance the valve travels from neutral or a "zero" reference.
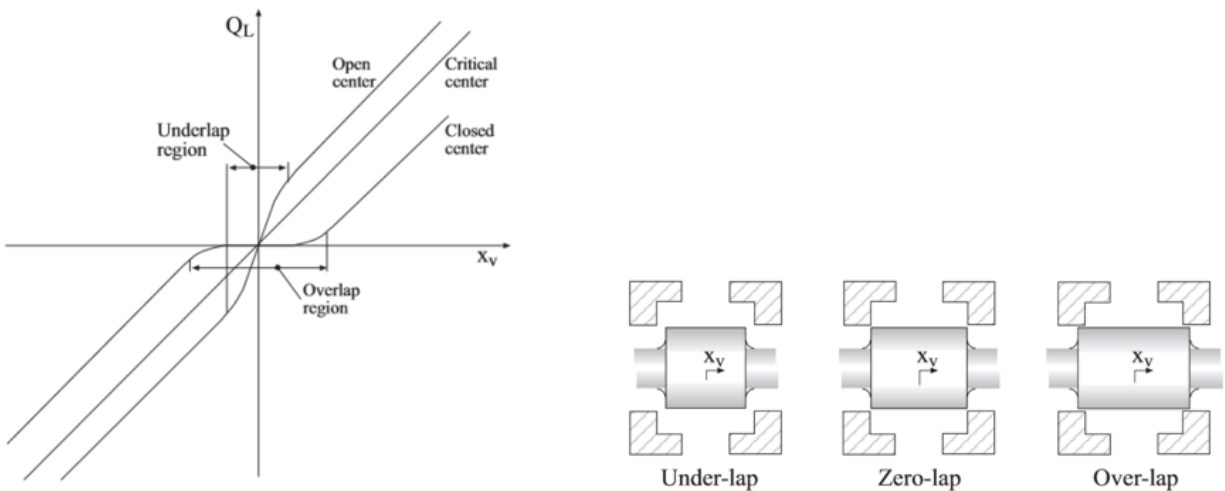
Figure 1.3:(Left) Flow vs. spool position gain & (Right) valve center types [1]

The EHSV in this study is a four-land four-port configuration with an over-lap center type. See the picture of the model below.
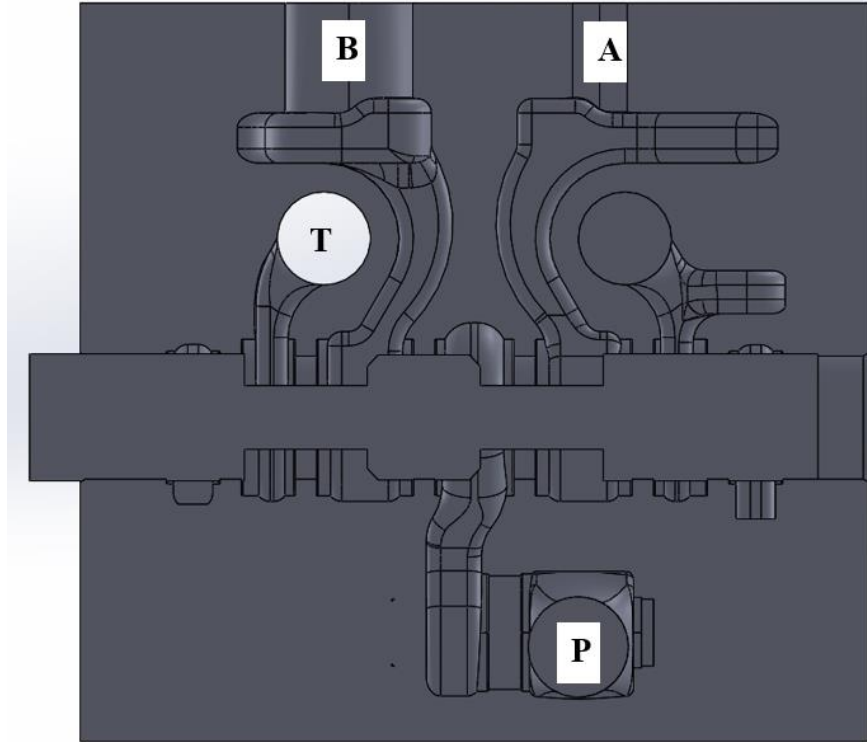
Figure 1.4: Picture of study valve
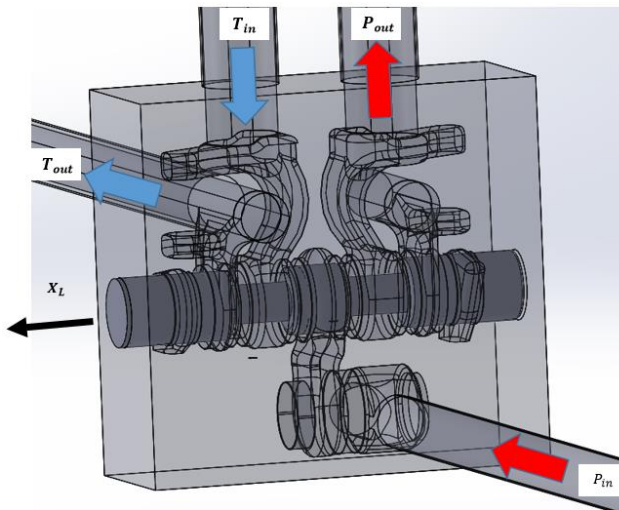
Figure 1.5: Flow paths
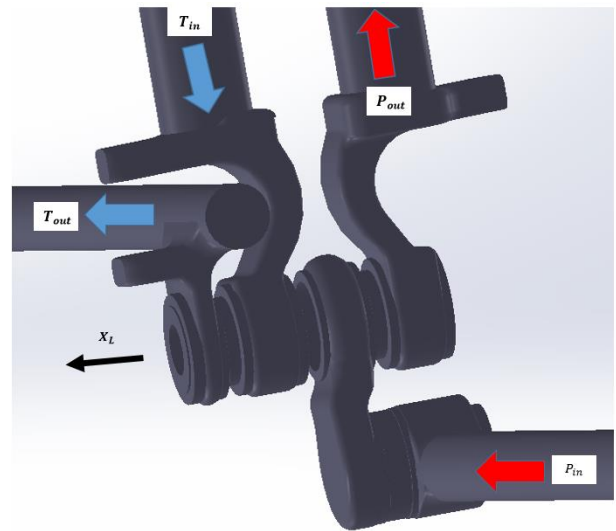
Figure 1.6: Extruded volume full valve stroke Steady-State model

1.2 Applications

The EHSV was developed in military applications such as a positioning mechanism in missile systems developed by Siemens corp. in Germany, Pre-World War II [2]. These systems used position feedback sensors to adjust a cylinder position and keep equipment level. These systems led to the development of servo valves used on modern aircraft to control fuel flow out of nozzles into turbines and control the position of lift and drag devices on the wing. Developments in the aerospace and military sectors created simple and lightweight valves that are now used across many other industries today [2].

1.3 Objectives

1. Calculate flow parameters including flow rate, static pressure, vorticity and turbulence quantities for a four-land four-port EHSV under SS and TR conditions for a range of valve stroke.

2. Perform a critical analysis of flow parameters including flow rate, static pressure, vorticity and turbulence quantities for a four-land four-port EHSV under steady-state and transient conditions for a range of valve stroke.

3. Perform a critical analysis of flow rate as measured on an experimental system.

In this thesis, flow through a closed-center (Figure 3) four-land four-port (Figure 2) EHSV is analyzed using both SS and TR simulations. Availability of computational power provides several different methods to model fluid flow. Unlike many previous studies, this thesis focuses on investigating the accuracy and consistency of computational models in order to improve fluids system design that included these types of valves [3, 4, 5]. This study compares simulation results at various points during valve stroke using SS and TR models. Measurements were taken

on an experimental setup to determine appropriate boundary conditions and compared to the simulated results to determine accuracy.

This thesis seeks to determine the necessary complexity of the model in order to model transient effects in a valve. Using a model created with SOLIDWORKS®, a common valve type was used to run a series of simulations utilizing different modeling setups. The results from these simulations were analyzed using VisIt post-processing software. Examination of the results includes flow, pressure, vorticity, and turbulent quantities. The goal of this thesis is to offer a quicker and cheaper design path for engineers to validate and implement utilizing CFD software.

1.4 Literature Review

A literature review was performed for studies analyzing flow through an EHSV. The studies found for EHSV modeling and simulations utilize primarily discrete SS methods to determine flow parameters at various valve openings. Studies found utilizing TR simulation were different valve types including a check and relief type.

Rigola (2015) [11] performed a study on an EHSV opening and uses discrete SS simulations to calculate flow at various time steps consistent with the methods used in this thesis. The goal of this study was to analyze turbulent flow through this valve utilizing different spool geometries.

Pan (2011) [12] utilizes discrete SS simulations to analyze the discharge characteristics of turbulent and laminar flow through an EHSV. This study developed a numerical model for discharge coefficients on an experimental setup.

Huang (2011) [13] also investigates the discharge characteristics of an EHSV at various pressures and flow rates to analyze and optimize a particular spool geometry.

Boqvist (2016) [15] investigates a check valve as it closes using a TR simulation. The author uses a dynamic mesh to extract forces at the valve induced by the flow.

Studies found evaluating EHSV were simulated using discrete SS simulations across valve stroke. This study is different from those previously done as it evaluates the difference between SS and TR models.

Chapter 2 Theoretical Background

Modeling flow requires the use of equations for the conservation of mass and momentum.

Turbulent flow requires additional scalar equations which are a derivation of the Navier-

Stokes Equation using the standard k-ε turbulence method.

Mass Conservation Equation: [10]

$$\frac{\partial \rho}{\partial t} + \nabla \cdot (\rho V) = 0 \qquad \qquad \textit{Equation 2.1}$$

Assuming incompressible flow:

$$\nabla \cdot V = 0 \qquad \qquad \textit{Equation 2.2}$$

Conservation of Momentum: [19]

$$\rho g_x - \frac{\partial p}{\partial x} + \frac{\partial \tau_{xx}}{\partial x} + \frac{\partial \tau_{yx}}{\partial y} + \frac{\partial \tau_{zx}}{\partial z} = \frac{\partial \rho u}{\partial t} + u\frac{\partial \rho u}{\partial x} + v\frac{\partial \rho u}{\partial y} + w\frac{\partial \rho u}{\partial z} \qquad \textit{Equation 2.3}$$

$$\rho g_y - \frac{\partial p}{\partial y} + \frac{\partial \tau_{xy}}{\partial x} + \frac{\partial \tau_{yy}}{\partial y} + \frac{\partial \tau_{zy}}{\partial z} = \frac{\partial \rho v}{\partial t} + u\frac{\partial \rho v}{\partial x} + v\frac{\partial \rho v}{\partial y} + w\frac{\partial \rho v}{\partial z} \qquad \textit{Equation 2.4}$$

$$\rho g_z - \frac{\partial p}{\partial z} + \frac{\partial \tau_{xz}}{\partial x} + \frac{\partial \tau_{yz}}{\partial y} + \frac{\partial \tau_{zz}}{\partial z} = \frac{\partial \rho w}{\partial t} + u\frac{\partial \rho w}{\partial x} + v\frac{\partial \rho w}{\partial y} + w\frac{\partial \rho w}{\partial z} \qquad \textit{Equation 2.5}$$

Using assumptions:

- Incompressible Flow
- Newtonian Fluid
- Flow is in a place normal to gravitational forces (g is negligible)
- Constant Properties

$$\tau_{xx} = 2\mu\frac{\partial u}{\partial x}; \quad \tau_{yy} = 2\mu\frac{\partial v}{\partial y}; \quad \tau_{zz} = 2\mu\frac{\partial w}{\partial z} \qquad \textit{Equation 2.6}$$

$$\tau_{xy} = \tau_{yx} = \mu(\frac{\partial u}{\partial y} + \frac{\partial v}{\partial x}) \qquad \textit{Equation 2.7}$$

$$\tau_{xz} = \tau_{zx} = \mu(\frac{\partial w}{\partial x} + \frac{\partial u}{\partial z}) \qquad \textit{Equation 2.8}$$

$$\tau_{yz} = \tau_{zy} = \mu(\frac{\partial v}{\partial z} + \frac{\partial w}{\partial y}) \qquad \textit{Equation 2.9}$$

Equations 2.3, 2.4 and 2.5 simplify to:

$$\mu\left(\frac{\partial^2 u}{\partial x^2} + \frac{\partial^2 u}{\partial y^2} + \frac{\partial^2 u}{\partial z^2}\right) = \rho\frac{\partial u}{\partial t} + \frac{\partial p}{\partial x} \qquad \textit{Equation 2.10}$$

$$\mu\left(\frac{\partial^2 v}{\partial x^2} + \frac{\partial^2 v}{\partial y^2} + \frac{\partial^2 v}{\partial z^2}\right) = \rho\frac{\partial v}{\partial t} + \frac{\partial p}{\partial y} \qquad \textit{Equation 2.11}$$

$$\mu\left(\frac{\partial^2 w}{\partial x^2} + \frac{\partial^2 w}{\partial y^2} + \frac{\partial^2 w}{\partial z^2}\right) = \rho\frac{\partial w}{\partial t} + \frac{\partial p}{\partial z} \qquad \textit{Equation 2.12}$$

The transport equations for the standard k-ε turbulence model is: [10]

$$\frac{\partial k}{\partial t} + \nabla(uk) = \nabla\left(\frac{v_T}{\sigma_k}\nabla k\right) + P - D \qquad \textit{Equation 2.13}$$

And:

$$\frac{\partial \varepsilon}{\partial t} + \nabla(u\varepsilon) = \nabla\left(\frac{v_T}{\sigma_\varepsilon}\nabla\varepsilon\right) + \frac{\varepsilon}{k}(C_{\varepsilon 1}P - C_{\varepsilon 2}D) \qquad \textit{Equation 2.14}$$

Where the production term P is

$$P = 2v_T\nabla(u^2) + v_T(\nabla u)^2 \qquad \textit{Equation 2.15}$$

Reynolds number (Re) is calculated using Equation 2.16

$$Re = \frac{\rho vd}{\mu} \qquad \textit{Equation 2.16}$$

Entrance lengths used in the simulation were calculated using the entrance length equations for

turbulent flow. *Reynolds numbers* greater than 4000 are considered turbulent. Equations for

laminar (2.17) [16], transitional (2.18) [17] and Turbulent (2.19) [7] entrance lengths can be seen

below.

$$\frac{L}{d} = [0.619^{1.6} + 0.0567Re^{1.6}]^{\frac{1}{1.6}} \qquad \textit{Equation 2.17}$$

$$\frac{L}{d} = \frac{2166718}{Re^{5/4}} \qquad \textit{Equation 2.18}$$

$$\frac{L}{d} = 4.4Re^{1/6} \qquad \textit{Equation 2.19}$$

Chapter 3 Numerical Methods

This chapter will identify the setting used while utilizing a CFD software, Ansys Fluent®, which is a module within Ansys Workbench® version 16.1. Geometry was produced using SOLIDWORKS® 2017 and meshed utilizing the Fluent® meshing tool within Workbench®. The standard k-ε turbulence method has been used on all simulations.

3.1 Fluent® Solution Techniques

The models enabled for all simulations in this study were the standard k-ε turbulence model. Though flow in the entrance and exit lengths is laminar, turbulent effects can be seen through the small openings in the valve. For simulations having difficulty converging, first order and linear solutions were run to calculate initial values. Turbulent second order solutions were then run to convergence.

3.1.1 Pressure Based Solver

ANSYS Fluent utilizes a technique that divides the domain into a discrete set of control volumes, called a mesh. The solver then integrates the governing equations to solve for each discrete dependent variable including velocity, pressure, temperature, and conserved scalars such as turbulent quantities.

3.1.2 Coupled Pressure Based Solver Algorithm

The coupled algorithm solves momentum and pressure equations simultaneously. This step increases the required memory of a process by 1.5 to 2 times, while decreasing total computation time. The segregated algorithm solves the momentum and pressure equations sequentially only requiring Fluent® to store one set of data hence the lower requirement for memory and the longer computation time.

3.1.3 Gradient Evaluation: Least Squares Method

The least squares cell based gradient method assumes that the solution varies linearly between each cell. It is especially efficient in evaluating meshes that have a relatively high skew and distortion. This method takes the geometric weight of each neighboring cells and applies that weight to the variable the gradient is being evaluated for. Due to its computational efficiency and accuracy Ansys® Fluent® uses this as its default setting.

3.1.4 Gradient Limiters: Second Order Upwind

This study utilizes the second order upwind method as gradient limiters. Gradient limiters are used to control oscillations while the simulation is solving by keeping the solution monotonic [6].

3.1.5 Second Order Pressure Interpolation Scheme

Default Ansys® Fluent® settings assume wall pressure gradients are zero, which is a source for error in systems with complex curvature at the walls. The default scheme interpolates the pressure values at faces using calculated momentum equation coefficients, which is accurate if transitions between the cell centers is smooth.

The second-order scheme sums the previously calculated cell face value and the product of the gradient. This method requires the solver to find the gradient of each face value in the mesh. The second order scheme has difficulty initializing with a complex mesh, which is why this study initializes with a linear scheme and then converges with the more accurate second order scheme.

3.1.6 Explicit Under-Relaxation

Explicit under relaxation sums the current cell face value and calculates the product of the under-relaxation factor and the gradient, providing a new value. This method assists in convergence by dampening oscillations in the solution. The under-relaxation factor used in this study was 0.5.

3.1.7 Iterative Time Advancement Scheme

To model TR simulations Ansys® Fluent® defaults to the iterative time advancement scheme. In this scheme the coupled algorithm is utilized at each time step. Once the solution converges at a time step it iterates to the next time step using the values from the previous as initial values.

3.2 Fluent® Processing

Flows within Ansys® Fluent® solve the conservation equations for both mass and momentum. Equations in this chapter all use the nomenclature of Fluent's® Theory Guide [6] rather than the nomenclature otherwise established for this document.

Continuity Equation: [6]

$$\frac{\partial \rho}{\partial t} + \nabla \cdot (\rho \vec{v}) = 0 \qquad \qquad \textit{Equation 3.1}$$

Momentum Conservation: [6]

$$\frac{\partial}{\partial x}(\rho \vec{v}) + \nabla \cdot (\rho \vec{v} \vec{v}) = -\nabla p + \nabla \cdot (\bar{\bar{\tau}}) + \rho \vec{g} + \vec{F} \qquad \textit{Equation 3.2}$$

Where the stress tensor,

$$\bar{\bar{\tau}} = \mu [(\nabla \vec{v} + \nabla \vec{v}^T) - \frac{2}{3} \nabla \cdot \vec{v} I] \qquad \qquad \textit{Equation 3.3}$$

The turbulence model used in this study is the standard k-ε turbulence method which calculates the *turbulent kinetic energy (TKE), k,* and the *rate of TKE dissipation, ε*, as follows. [6]

$$\frac{\partial}{\partial t}(\rho k) + \frac{\delta}{\delta x_i}(\rho k u_i) = \frac{\delta}{\delta x_j}\left[\left(\mu + \frac{\mu_t}{\sigma_k}\right)\frac{\delta k}{\delta x_j}\right] + G_k - \rho \varepsilon \qquad \text{Equation 3.4}$$

And

$$\frac{\partial}{\partial t}(\rho \varepsilon) + \frac{\delta}{\delta x_i}(\rho \varepsilon u_i) = \frac{\delta}{\delta x_j}\left[\left(\mu + \frac{\mu_t}{\sigma_\varepsilon}\right)\frac{\delta \varepsilon}{\delta x_j}\right] + C_{1\varepsilon}\frac{\varepsilon}{k}(G_k) - C_{2\varepsilon}\rho\frac{\varepsilon^2}{k} \qquad \text{Equation 3.5}$$

Where G_k represents the turbulent kinetic energy due to mean velocity gradients.

The modeling constants above are defined values for the standard k-ε turbulence method, which have been shown to work well with a wide range of wall bounded flows. [6]

$$C_{1\varepsilon} = 1.44, \qquad C_{2\varepsilon} = 1.92, \qquad C_\mu = 0.09, \qquad \sigma_k = 1.0, \qquad \sigma_\varepsilon = 1.3$$

3.3 Convergence Criterion

Various levels of convergence criteria levels are used across industry, but all typically are evaluated by the value of the simulations residuals (lower is better). A residual is the error produced when attempting to balance the governing equations. Fluent® then scales these residuals using the flow through that specific element. The sum of these scaled residuals is then reported for each iteration.

Typically, computation time is the limit to the level of convergence that can be acquired. For the purposes of this study, residual values on the order of 10^{-3} are considered qualitative, values on the order of 10^{-5} are considered moderately converged and residuals on the order of 10^{-6} are considered strongly converged. [9] Residual values and convergence are only trustworthy if the input parameters are accurate. All simulations in this study converged to 10^{-6} which indicate strong numerical accuracy relative to the quality of the boundary conditions.

Chapter 4 Methodology

The model was created in SOLIDWORKS®, then exported as a *step file* (Standard for the

Exchange of Product Data, ISO 10303) and imported into Ansys® Workbench® for meshing.

All activities requiring high performance computation such as meshing, and simulation were

performed on the Buddy Supercomputer Cluster at the University of Central Oklahoma. Buddy is

a 37-node cluster with 31 computer nodes, four high-memory nodes and two GPU nodes. Each

node has 20 CPUs and 64 GB of memory and each high memory node has 128GB of memory.

The limiting factors for each simulation was the 60 Fluent® licenses available for computation.

4.1 Simulation Set Up

In order to perform a critical analysis between SS and TR results, several SS simulations had to

be run at various valve strokes. The simulations analyze flow profiles from $1.25mm > X_L >$

$7.87mm$. The tables below show time and stroke intervals for each model type. TR simulations

run every 3ms for a total of 30 intervals. Utilizing a user defined function (UDF), valve stroke

position was adjusted according to simulation time. Simulation data has been obtained for each

of the cases shown above to perform the critical analysis.

Table 4-1: SS simulation settings

SS Intervals	Stroke (mm)	Time (ms)
0	1.54000	4.5
1	2.88000	22.5
2	4.54000	45.0
3	6.21000	67.5
4	7.87	90.0

Table 4-2: TR simulation settings (0-14)

TR Intervals	Stroke (mm)	Time (ms)
0	1.25	0
1	1.472	3
2	1.694	6
3	1.916	9
4	2.138	12
5	2.36	15
6	2.582	18
7	2.804	21
8	3.026	24
9	3.248	27
10	3.47	30
11	3.692	33
12	3.914	36
13	4.136	39
14	4.358	42

Table 4-3: TR simulation settings (15-30)

TR Intervals	Stroke (mm)	Time (ms)
15	4.58	45
16	4.802	48
17	5.024	51
18	5.246	54
19	5.468	57
20	5.69	60
21	5.912	63
22	6.134	66
23	6.356	69
24	6.578	72
25	6.8	75
26	7.022	78
27	7.244	81
28	7.466	84
29	7.688	87
30	7.87	90

4.1.1 Boundary Conditions

Boundary Conditions have been extrapolated from experimentally obtained pressures. See Chapter 5 for experimental setup and data. Inlet boundary conditions are shown in the table below:

Table 4-4: Simulation boundary conditions

P_{in}			T_{in}		
Gauge Total Pressure	12.47	Mpa	Gauge Total Pressure	1.675	Mpa
Initial Gauge Pressure	0	Mpa	Initial Gauge Pressure	0	Mpa
Direction	Normal		Direction	Normal	
Turbulent Intensity	5		Turbulent Intensity	5	
Turbulent Viscosity Ratio	10		Turbulent Viscosity Ratio	10	

P_{out}			T_{out}		
Gauge Total Pressure	9.025	Mpa	Gauge Total Pressure	0.2965	Mpa
Initial Gauge Pressure	0	Mpa	Initial Gauge Pressure	0	Mpa
Direction	Normal		Direction	Normal	
Turbulent Intensity	5		Turbulent Intensity	5	
Turbulent Viscosity Ratio	10		Turbulent Viscosity Ratio	10	

4.1.2 Working Fluid

The working fluid used in this study is ISO viscosity grade 32 hydraulic oil. The fluid properties are taken at 40°C with a *kinematic viscosity* of 30 cSt (3e-5 m^2/s) and 32 API (approximately 865 kg/m^3).

4.2 Model Specifications

The model consists of two flow paths or fluid regions. One represents high pressure fluid being sent to perform hydraulic work, while the other represents low pressure fluid returning to the fluid reservoir. *Entry* and *exit lengths* are 15.875mm in diameter, which match the geometry of the model and experimental system. The interior of the model has been designed to be very similar to the physical system, while the valve has been simplified for analysis in this study.

Below is a graphic (figure 5) showing the valve assembly and cavities, direction of flow and notation on inlets and outlets.
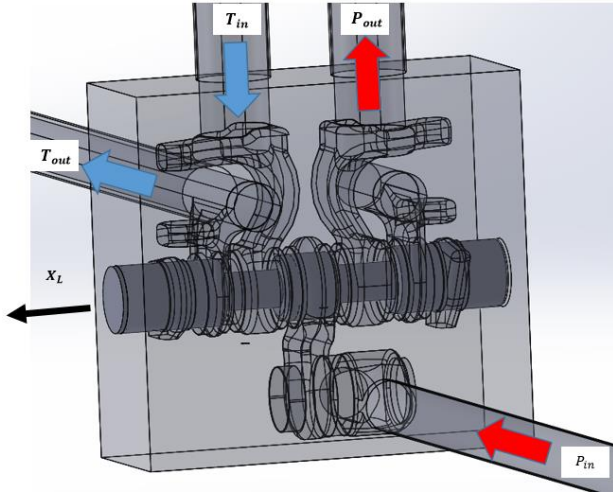
Figure 4.1: Flow paths
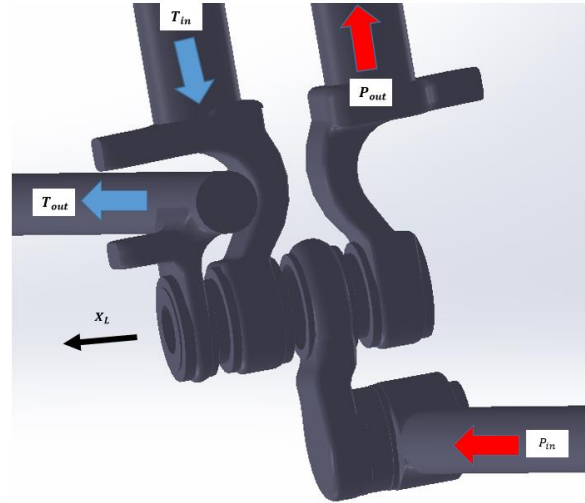
Figure 4.2: Extruded volume full valve stroke SS model

Entrance Lengths were chosen to be 1m to ensure fully developed flow at the valve entrance.

Using equation 2.19 (turbulent flow for entrance length), this is true for *Re* less than $8.92 \ (10^5)$.
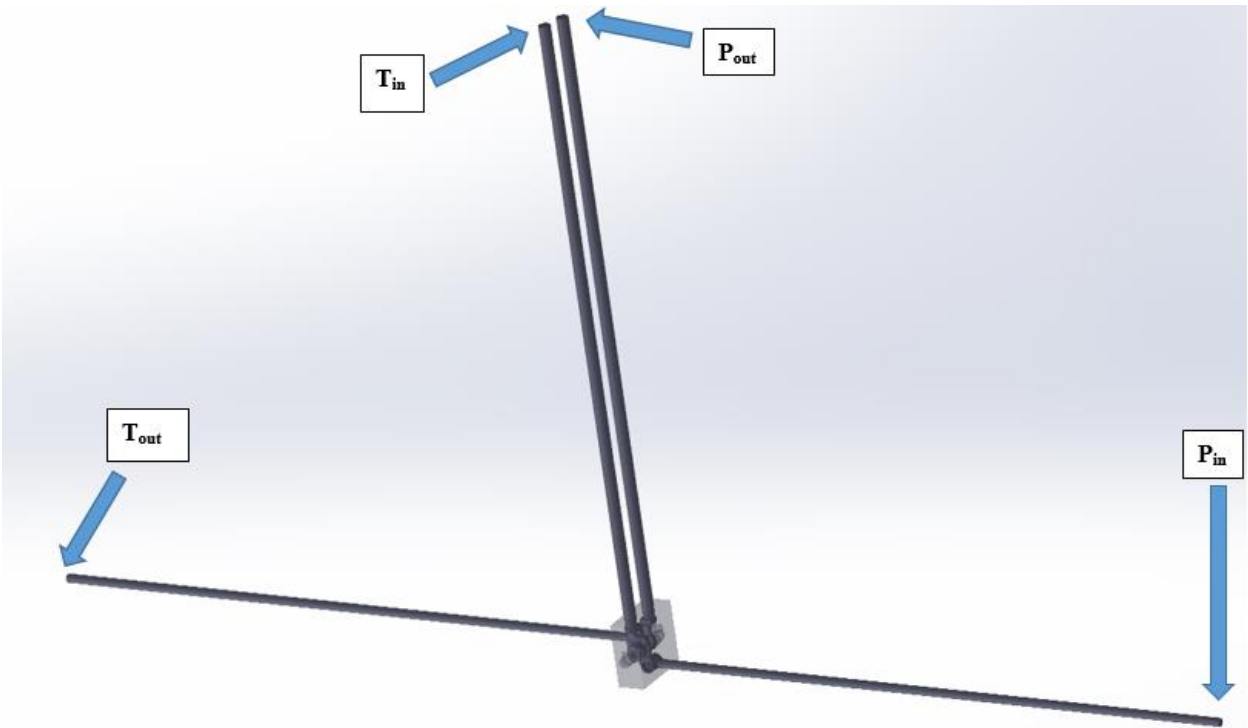
Figure 4.3: Boundary Surface locations

Below is the dimensions of the valve used in this study, all units are in mm. The exact valve used in the experimental system is a proprietary design, so a simplified linear spool was produced for the simulations.
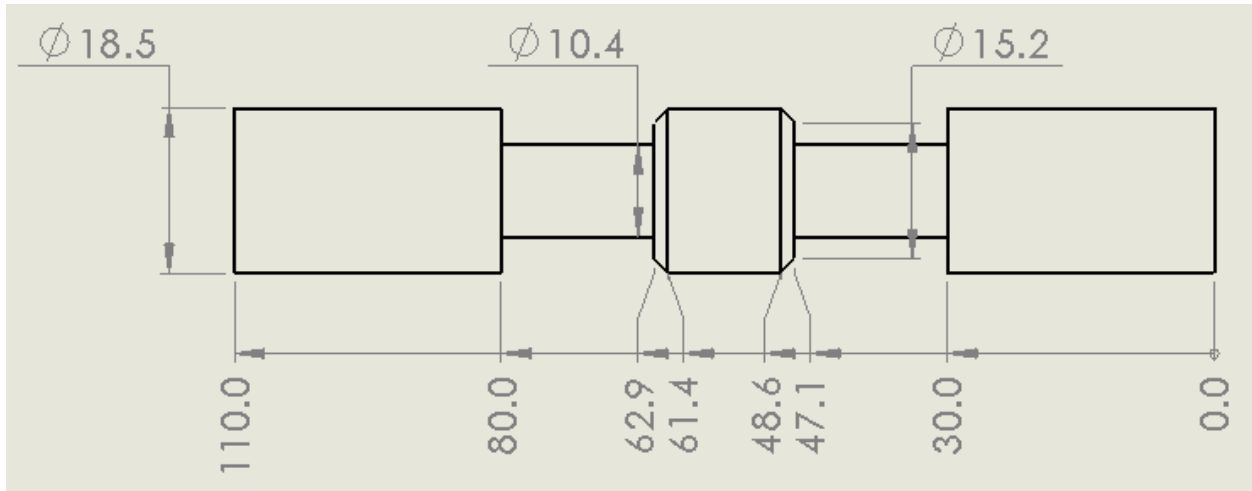
Figure 4.4: Valve spool dimensions (mm)

The type of valve modeled is a closed-center (Figure 1.3) four-land four-port (Figure 1.2) EHSV and was created using SOLIDWORKS 2017®. Once the solid valve was modeled, Ansys® SpaceClaim® was used to extract the fluids volume. Machined voids in the valve were inversely modeled for dynamic meshing.

Creating the model for the TR simulation required taking two separate SOLIDWORKS® models and appending them together in Ansys® Fluent®. Further details can be found in Appendix B for detailed setup of dynamic meshing zone for TR simulations.

Each SS model was modified for valve stroke and exported into a separate *step file* that was then important into Ansys® Fluent® for simulation. Meshing was performed by Ansys® Mechanical® to produce a mesh using default CFD settings. Post processing data was exported into *CGNS file* (CFD General Notation System, AIAA R-101A-2005) format. The data was then

imported into VisIT; which is a distributed, parallel visualization and graphical analysis tool [18].

4.3 Model Meshing

The geometry in this study is complex, with small machined cavities and sharp edges at transitions. Due to this complexity, the mesh is unstructured and consists of tetrahedral elements [20].

4.3.1 Steady-State Mesh Analysis

Meshing geometries are controlled by setting minimum and maximum edge size, allowing Ansys® to control element shape, which produced a tetrahedral mesh. In order to ensure simulation results were not dependent on mesh densities, five levels of varying mesh refinement were considered for each steady state model resulting in a total of 25 SS mesh refinements. Meshes with more than approximately $2(10^6)$ elements had flow values in the model remain constant. This level of refinement was then used for further calculations to reduce computation time.

The smallest valve opening, 1.54mm, has an initial drop in flow rate at the second level of mesh refinement. By taking a closer look at the mesh for the valve opening in this model in refinement two, only one element is present across the small opening in several places, which would lead to poor result quality. This can be seen below in
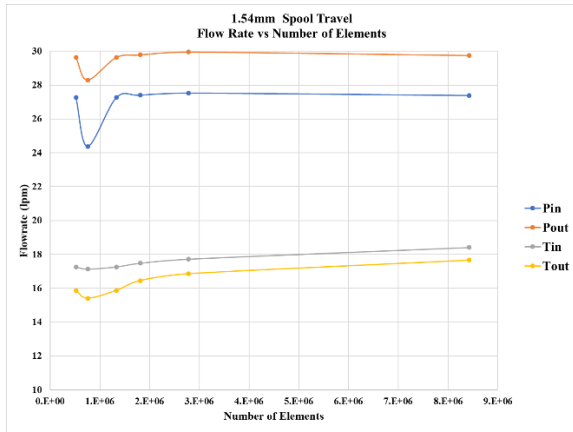
Figure 4.5: 1.54mm mesh refinement
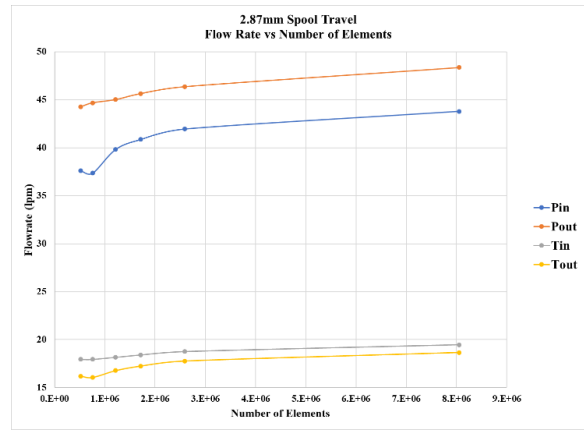
Figure 4.7: 2.87mm mesh refinement
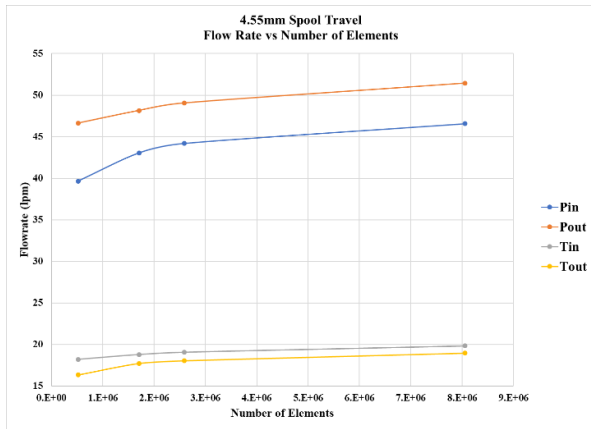
Figure 4.6: 4.55mm mesh refinement
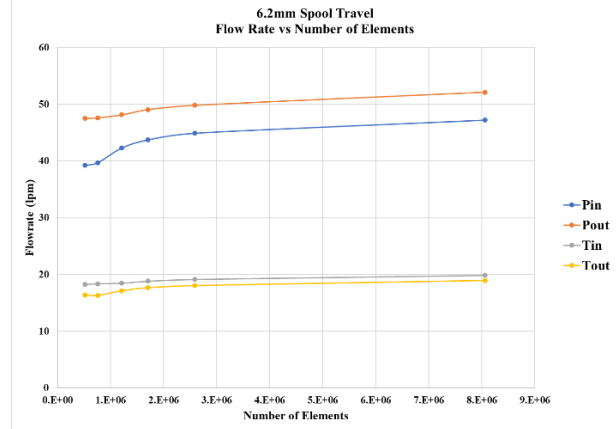
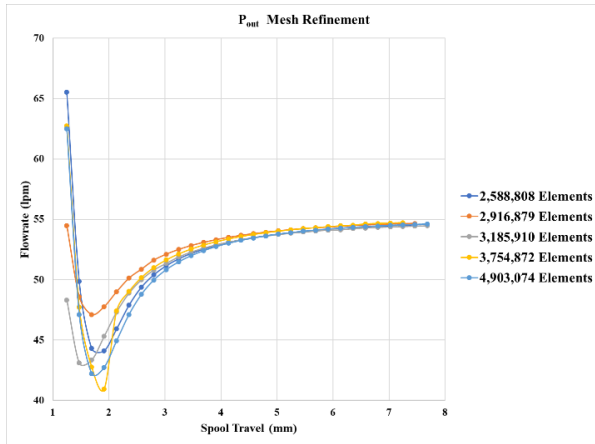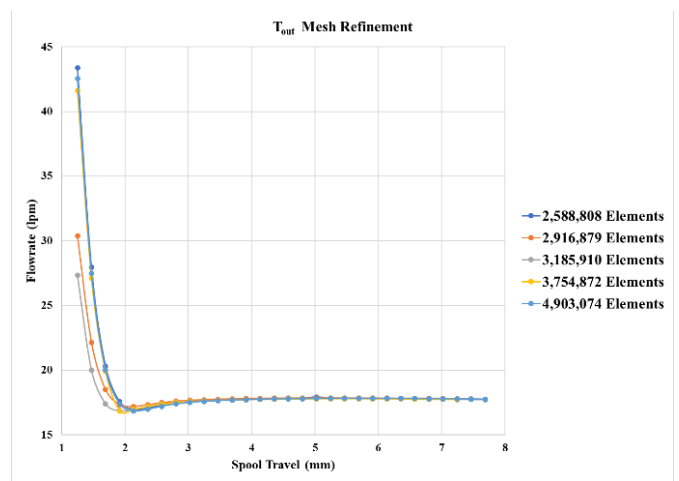*Figure 4.8: 6.2mm mesh refinement*
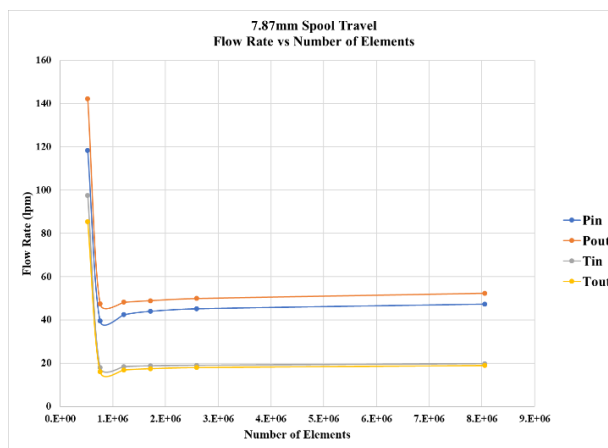
Figure 4.9: 7.87mm mesh refinement

20

Below are images of the coarsest and most refined mesh for the 1.54 mm valve stroke SS simulation.
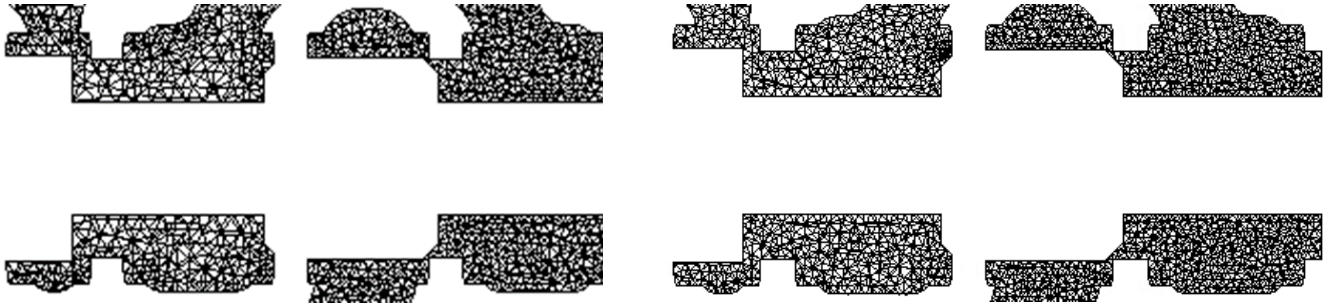
Figure 4.10: 1.54 mm stroke SS, 520,358 Elements

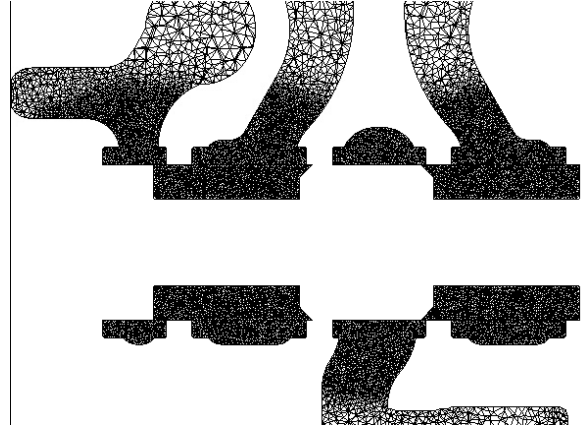Figure 4.11: 1.54 mm stroke SS, 8,055,950 Elements
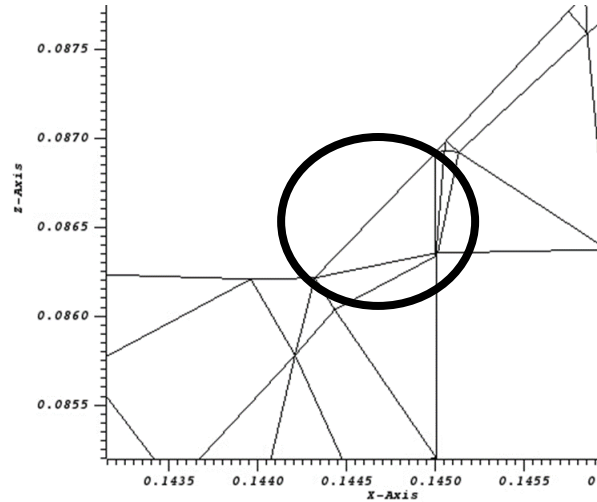
Figure 4.12: Valve opening gap 1.54mm mesh refinement two

4.3.2 Transient Mesh Analysis

The TR mesh refinement focused on the mesh around the valve movement. The dynamic mesh and the area where the mesh was to interface with the remaining portion of the valve was refined at the same size. Five refinements of the dynamic mesh were analyzed to ensure mesh density did not affect simulation results. The second finest refinement was chosen with approximately $4(10^6)$ elements. The initial spike in flow at low valve positions can also be attributed to the small gap when the valve is opening having only one element across it.

21
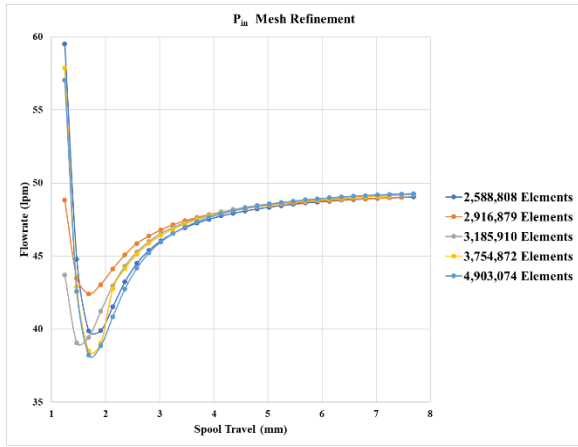
Figure 4.13: Pin mesh refinement
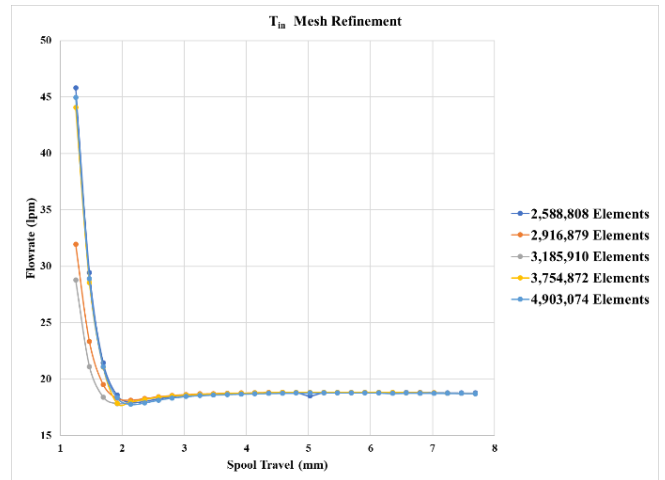
Figure 4.15: Tin mesh refinement

Figure 4.14: Pout mesh refinement

Figure 4.16: Pout mesh refinement

Below are images of the coarsest mesh and the most refined mesh for the 1.25 mm valve stroke TR simulation.
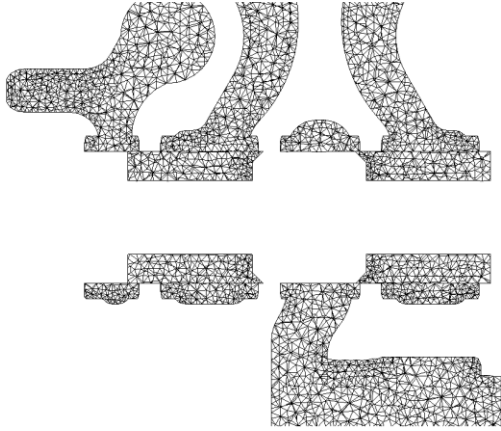
| Figure 4.17: TR 1.25mm valve stroke 2,588,808 elements | Figure 4.18: TR 1.25mm valve stroke 4,903,074 elements |

4.3.3 Mesh Motion

Mesh motion within the TR simulation was controlled with a user defined function, or UDF and can be found in appendix A. Valve motion was a linear function with a velocity of $0.074\frac{m}{s}$ and a valve opening time of 90 ms. Figure 4.19 below shows stroke versus time.
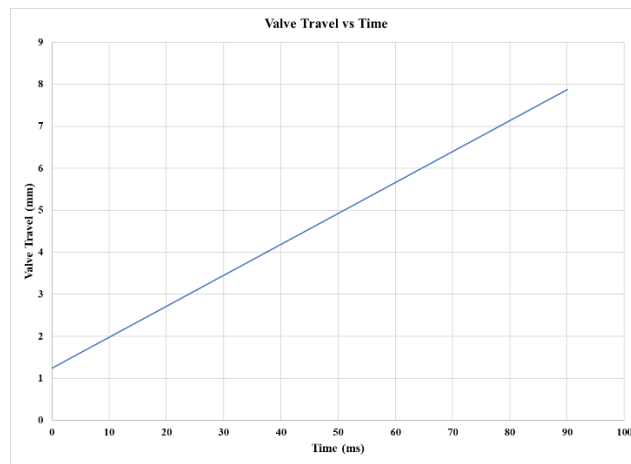
Figure 4.19: Spool travel vs time

4.3.4 Dynamic Mesh

The dynamic mesh was setup using a compiled user defined function, as stated above. Mesh quality along the valve interface was important, which is why cell sizing settings were identical

23

along the volume in the valve. A dynamic meshing event was set to initialize a change in movement assigned to the interior of the valve meshing portion shown in the figure below.
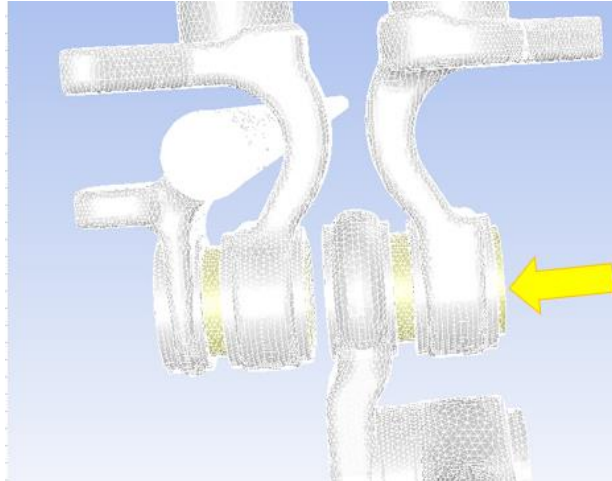
Figure 4.20: Dynamic mesh zone

Chapter 5 Experimental Setup

Experimental values were taken from a telehandler with a similar valve setup. Measured values include pressure, which were used to define boundary conditions and flow, which were used to evaluate simulation accuracy. The valve system used is made up of several EHSV connected in series. While taking measurements these valves were closed.

5.1 Piping and Instrumentation Diagram (P&ID)

Below is the P&ID for the experimental system where the dashed box designates the simulated system.
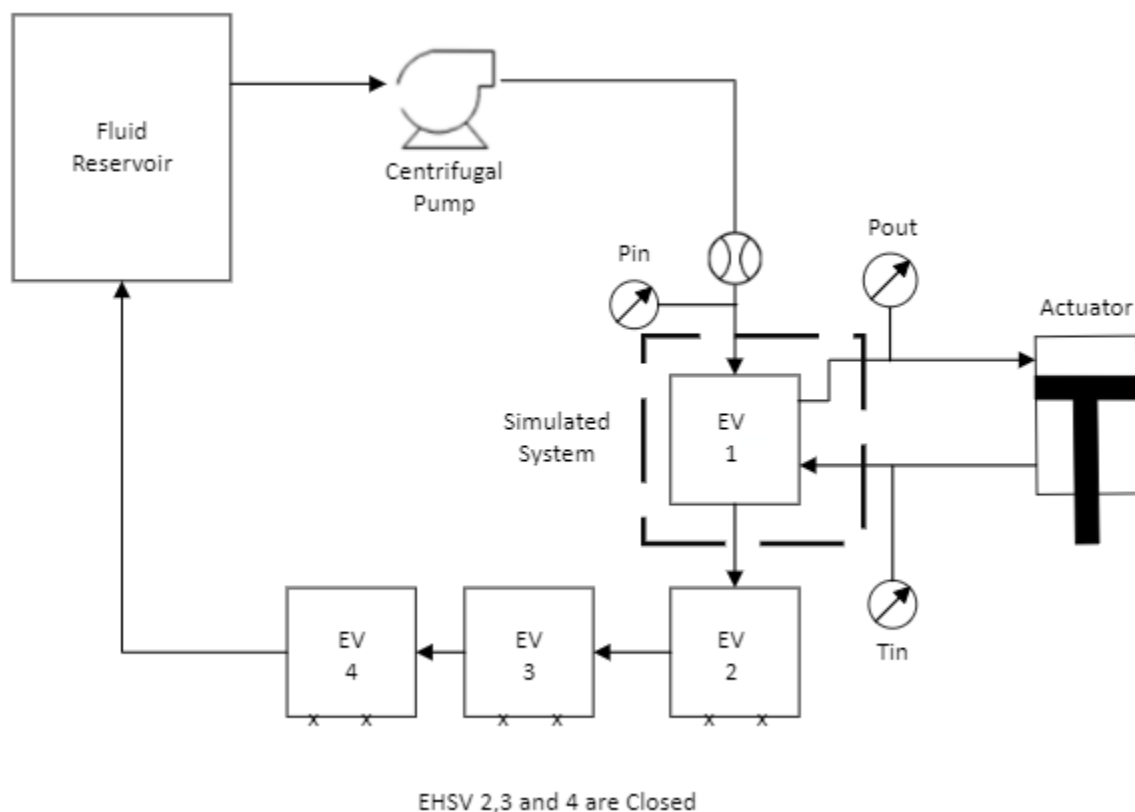
Figure 5.1: System P&ID

Gauges utilize a deformable diaphragm as a strain gauge to measure pressure. Flow is measured by a turbine-type flow meter at the entrance of the manifold. Sampling rate for the pressure and flow measurements is 100 hz. Accuracy of both devices is +/- 0.5%

5.2 Experimental Results

Below are the recorded values for simulation boundary conditions.
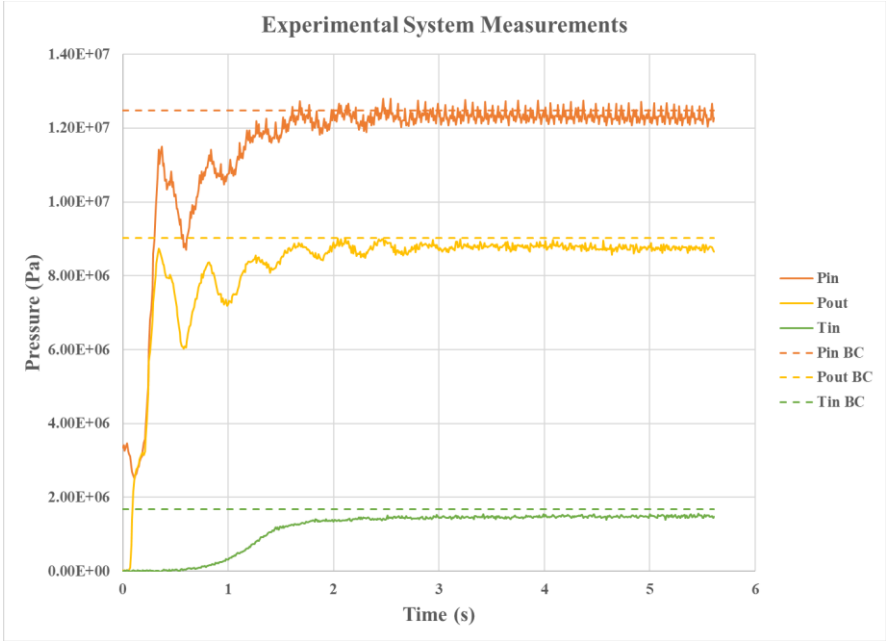
Figure 5.2: Experimental pressure measurements and BC

Below are the recorded values for experimental flowrate.
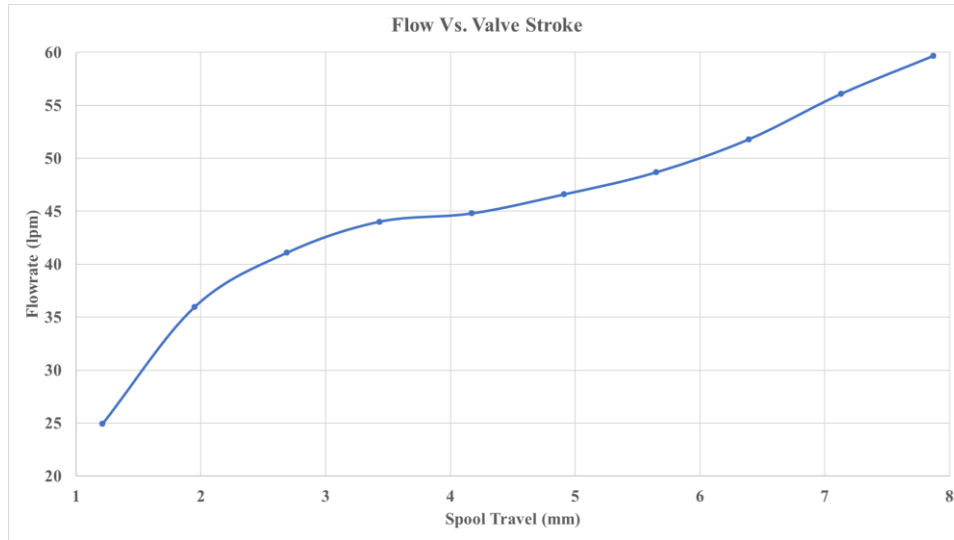
Figure 5.3: Experimental flow conditions

5.3 Simulation and Experimental Comparison

The simulation and experimental conditions are accurate enough for a qualitative and approximate numerical comparison. The pressure outlet and tank inlet boundary conditions in the simulation accurately represent the real system. Steady state values in the data were chosen for the constant pressure boundary conditions in the system. The flow rate was taken at the pressure inlet and measures the high-pressure flow rate into the valve. Overall, the results are an accurate representation of the flow parameters.

Chapter 6 Results

Results were taken and viewed on two planes in the simulation. The first is called half slice and is taken at the center of the valve. The second is a slice taken orthogonal to the spool in the pressure section of the valve. Both can be seen in the figure below.
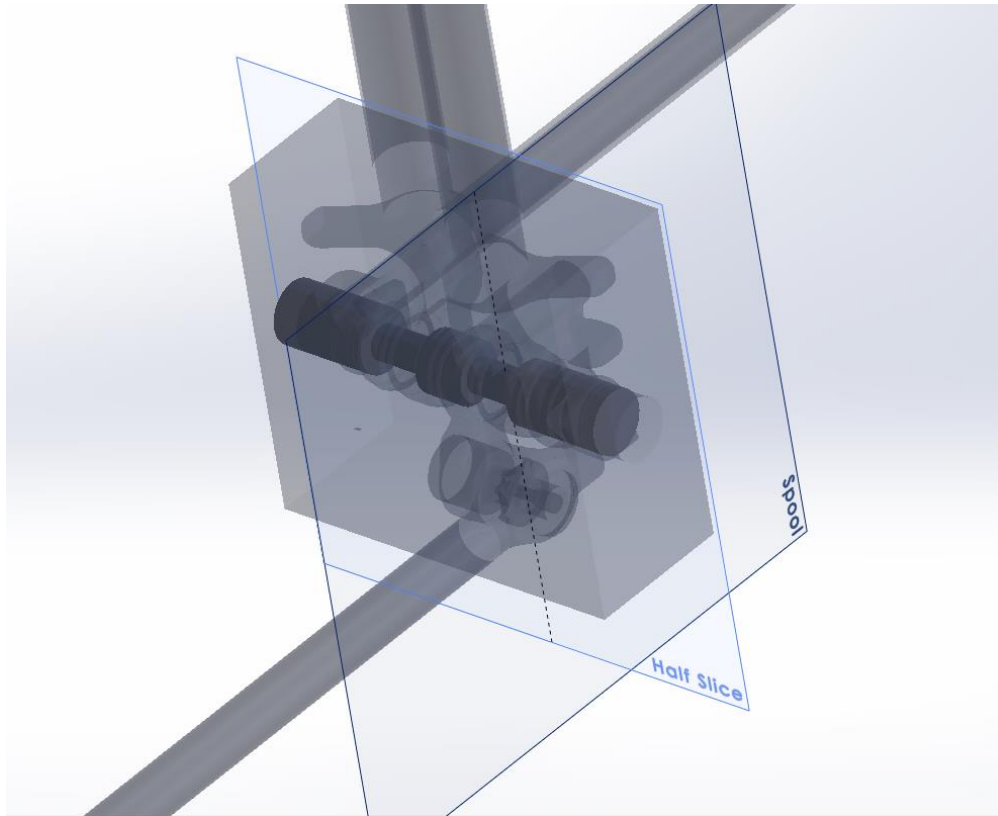
Figure 6.1: Contour plane locations

6.1 Simulation Flow Parameters

Experimental measurements are plotted below with simulation results on flow through the P_{in} surface. The dashed lines plotted to the (0 mm, 0 lpm) point are a projection, since the flow is known to be zero when it is closed.
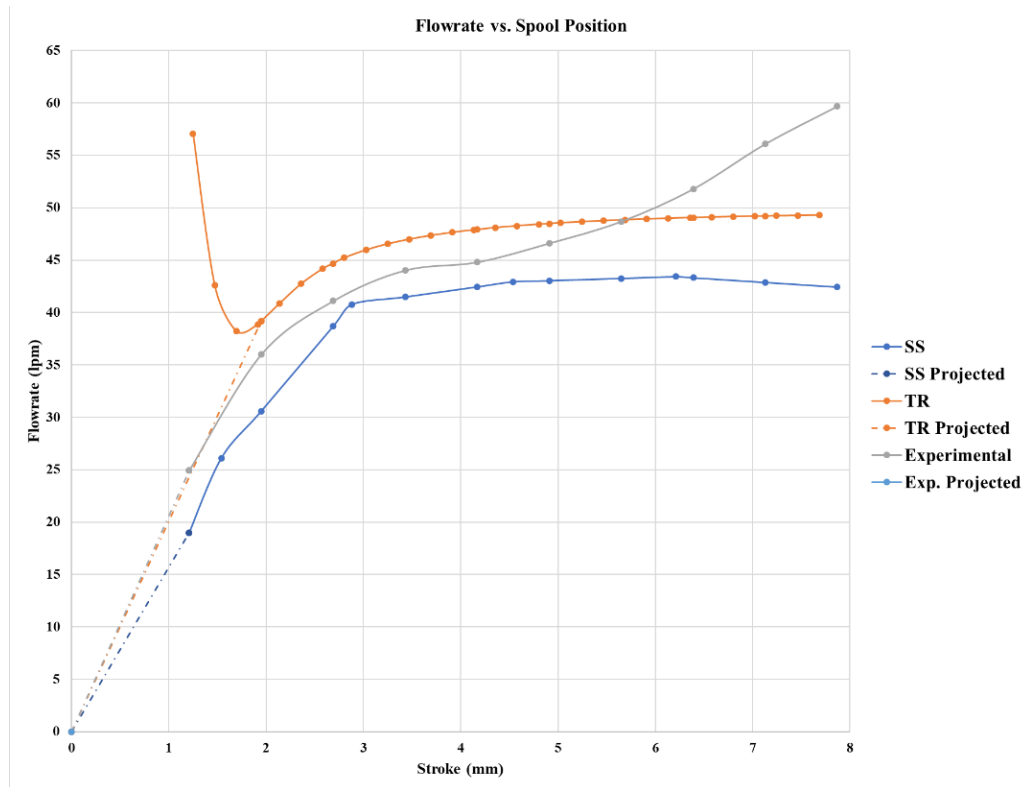
Figure 6.2: Simulation flow results

Pressure drop through the valve at various flowrates is a common quantity used in industry. The figure below shows the pressure drop across the two flow paths for the SS and TR simulations versus spool travel.
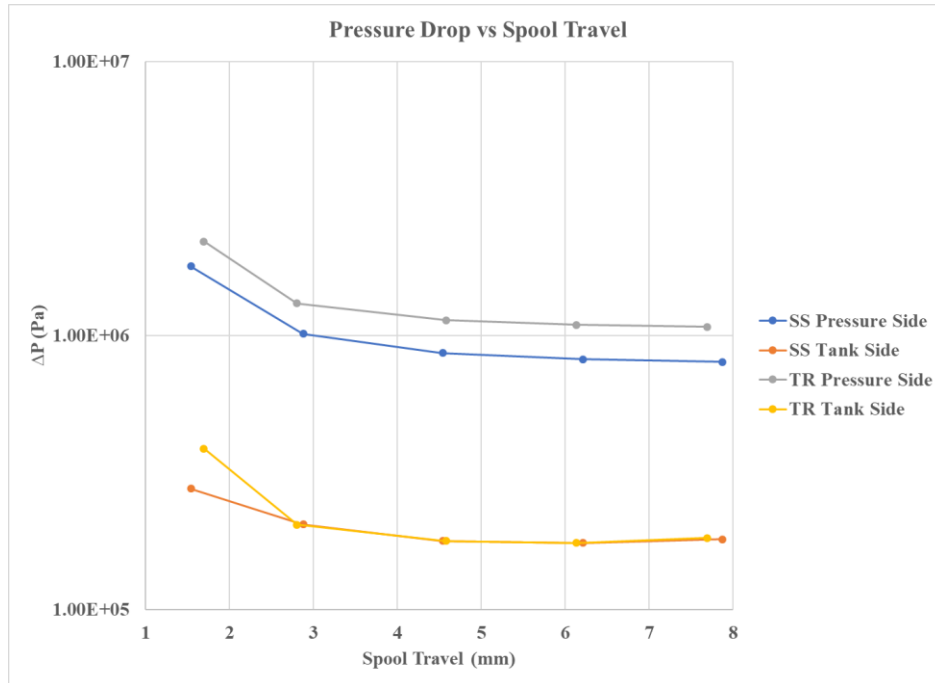
Figure 6.3: Pressure Drop vs Spool Travel

The figure below shows the maximum vorticity values across the valve for the SS and TR simulations versus spool travel. When the valve begins to open, the maximum vorticity is observed at the valve opening. As the valve opening and flow increase, the position where the maximum *vorticity* is found changes location. Vertical lines are placed when this phenomenon can be observed in each simulation. The stroke when this shift occurs happens at different locations along spool travel for each simulation.
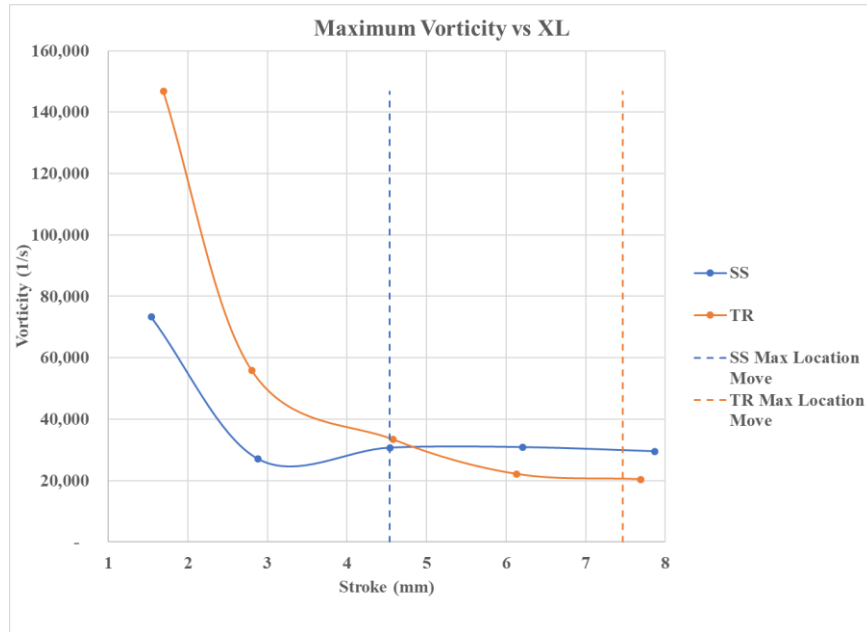
Figure 6.4: Maximum vorticity vs stroke

The figure below indicates the location where the maximum vorticity values are observed during
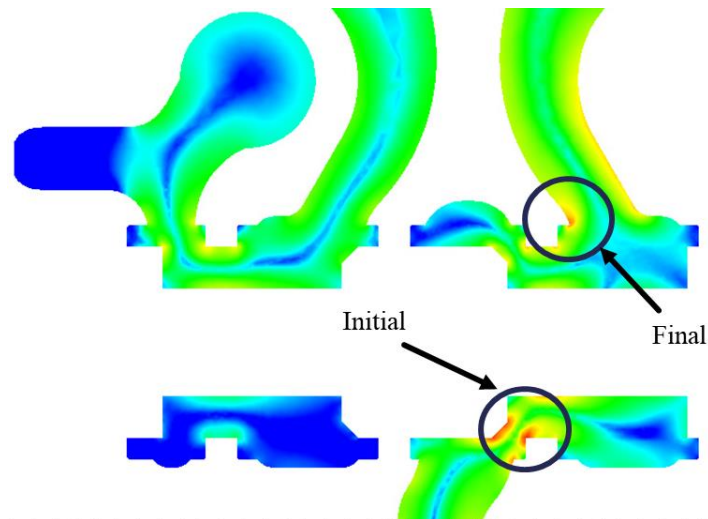
the simulation.

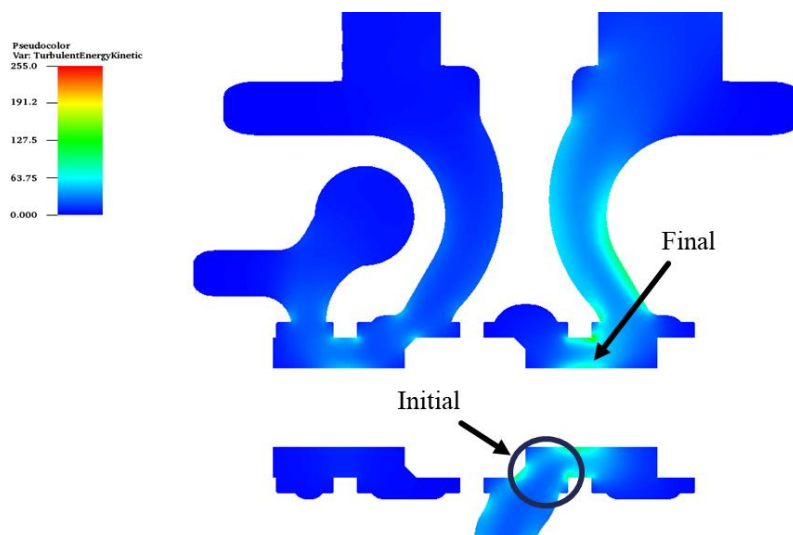*Figure 6.5: Maximum vorticity Locations*

The figure below shows the maximum *TKE* value across the valve for the SS and TR simulations

versus spool travel. When the valve begins to move, the maximum *TKE* can be found at the

opening . As the valve opens and flow increases, the position where the maximum vorticity is

observed changes location. Vertical lines are placed when this phenomenon occurs in each simulation.
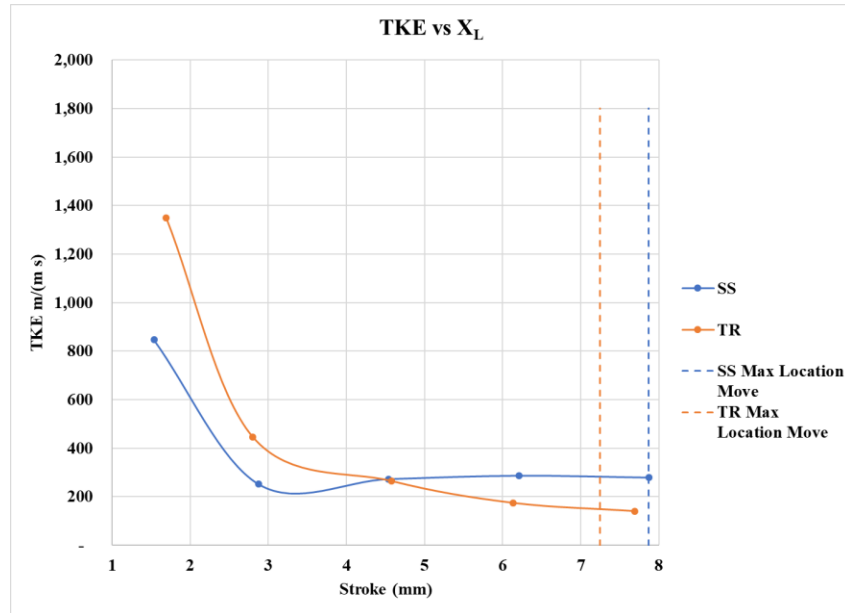
Figure 6.6: TKE vs stroke

The figure below indicates the location where the maximum *TKE* values are observed during the simulation.

Figure 6.7: Maximum TKE locations

The figure below shows the maximum *TKE dissipation rate* across the valve for the SS and TR simulations versus spool travel. The turbulence dissipates downstream out of the valve.
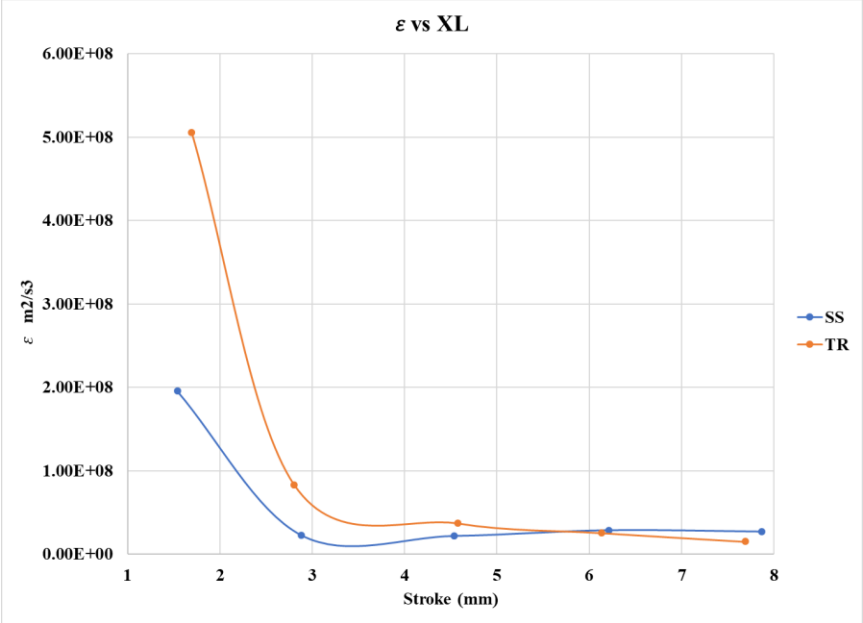
Figure 6.8: TKE dissipation rate vs stroke

6.2 Flow Field Contours

Flow field images are displayed sequentially for valve stroke in the SS and TR simulations. The images reflect *pressure, velocity* and *vorticity*

6.2.1 Static Pressure and Velocity Contours

Velocity vectors are plotted on the *pressure* contours below to illustrate flow through the EHSV at various stroke positions. Figures 6.9-18 show SS pressure and figures 6.19-28 show TR pressure contours both at half slice and spool planes.

6.2.1.1 SS Half Slice Contours
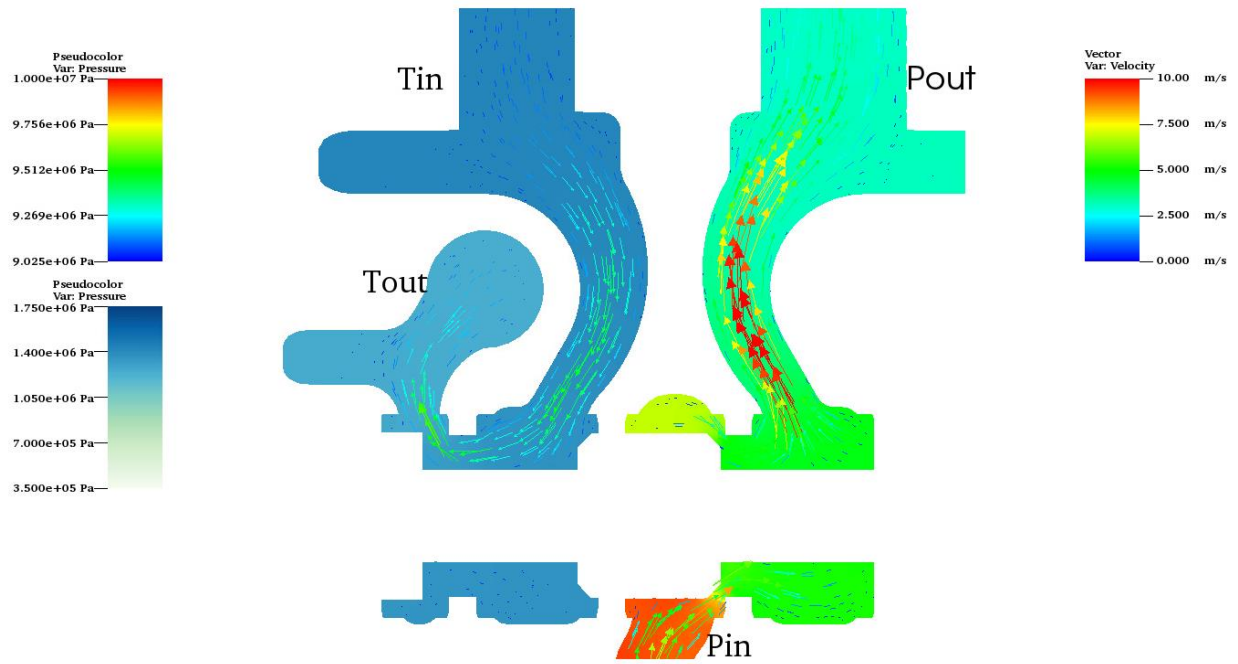
Figure 6.9: Pressure contour, velocity vectors, SS 1.54mm stroke half slice
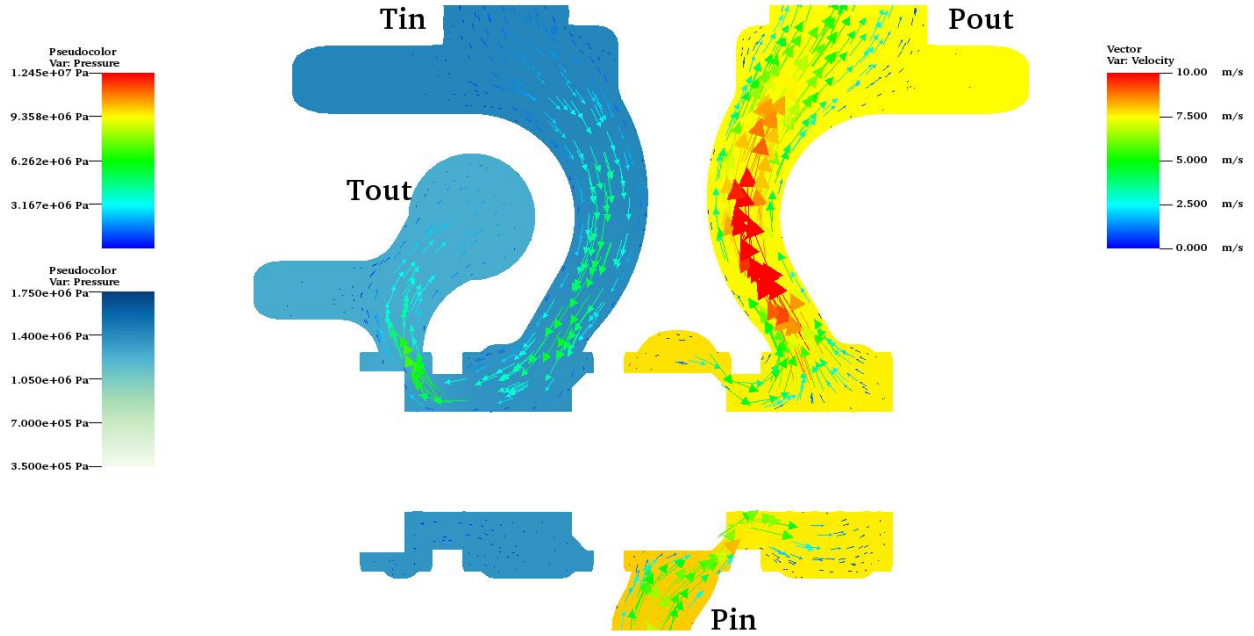
Figure 6.10: Pressure contour, velocity vectors, SS 2.88mm stroke half slice
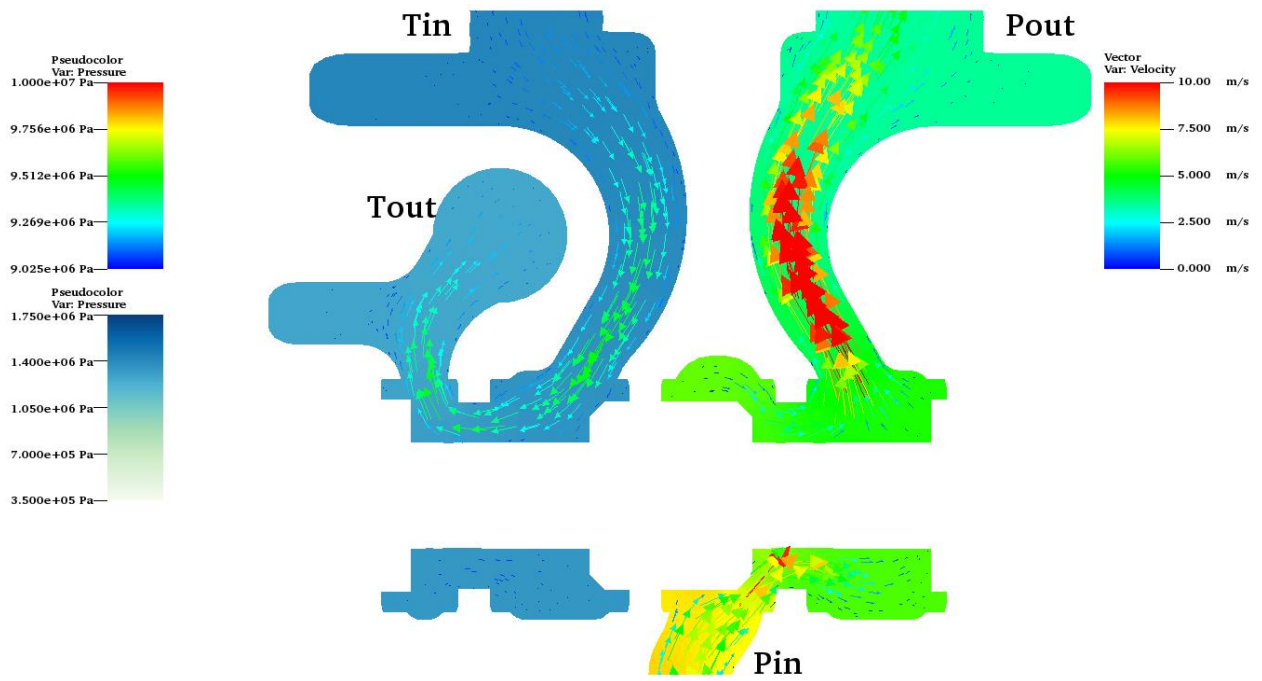
Figure 6.11: Pressure contour, velocity vectors, SS 4.54mm stroke half slice
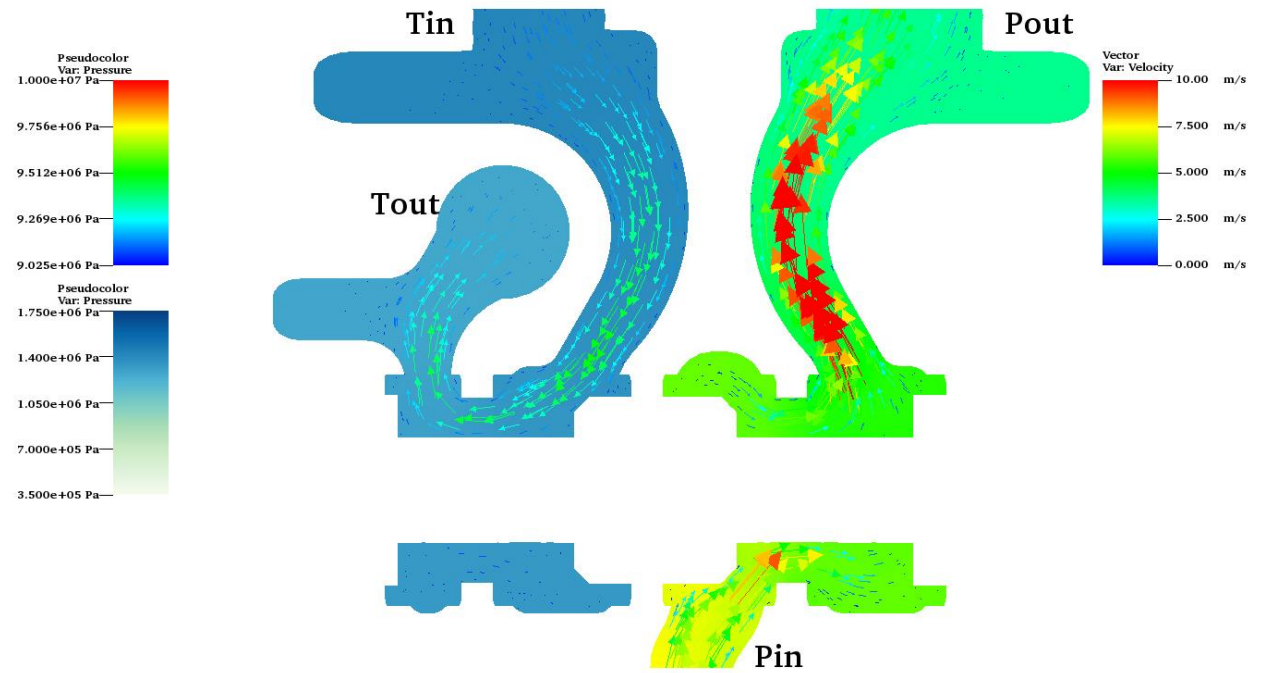

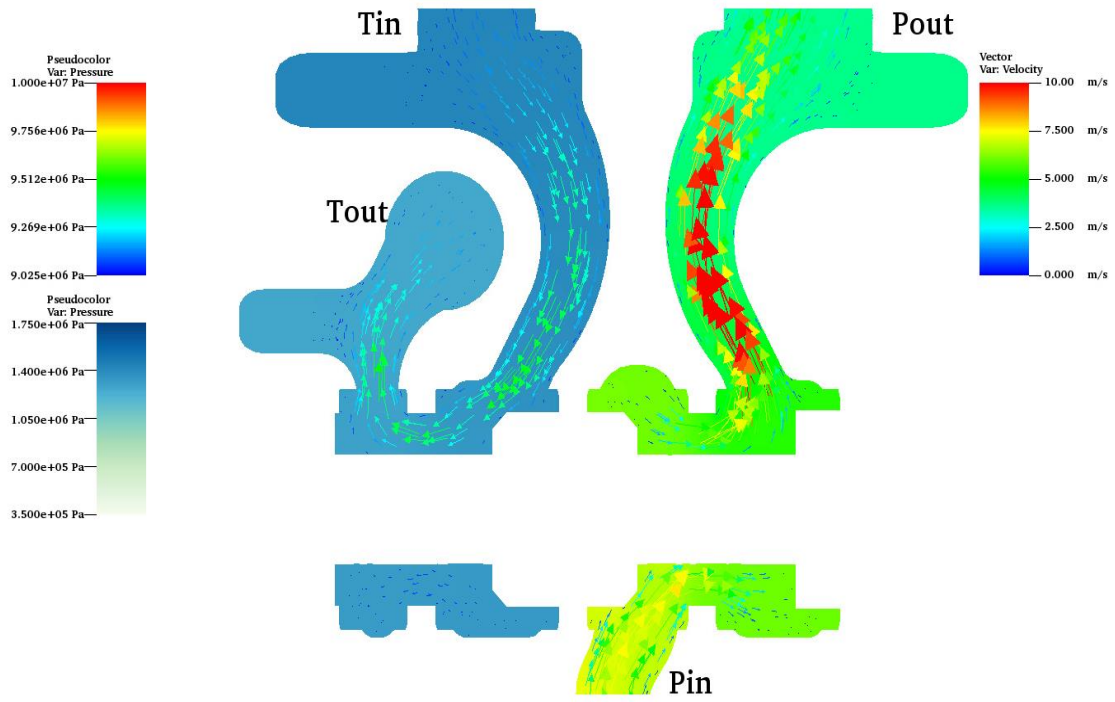*Figure 6.12: Pressure contour, velocity vectors, SS 6.21mm stroke half slice*

Figure 6.13: Pressure contour, velocity vectors SS 7.87mm stroke half slice
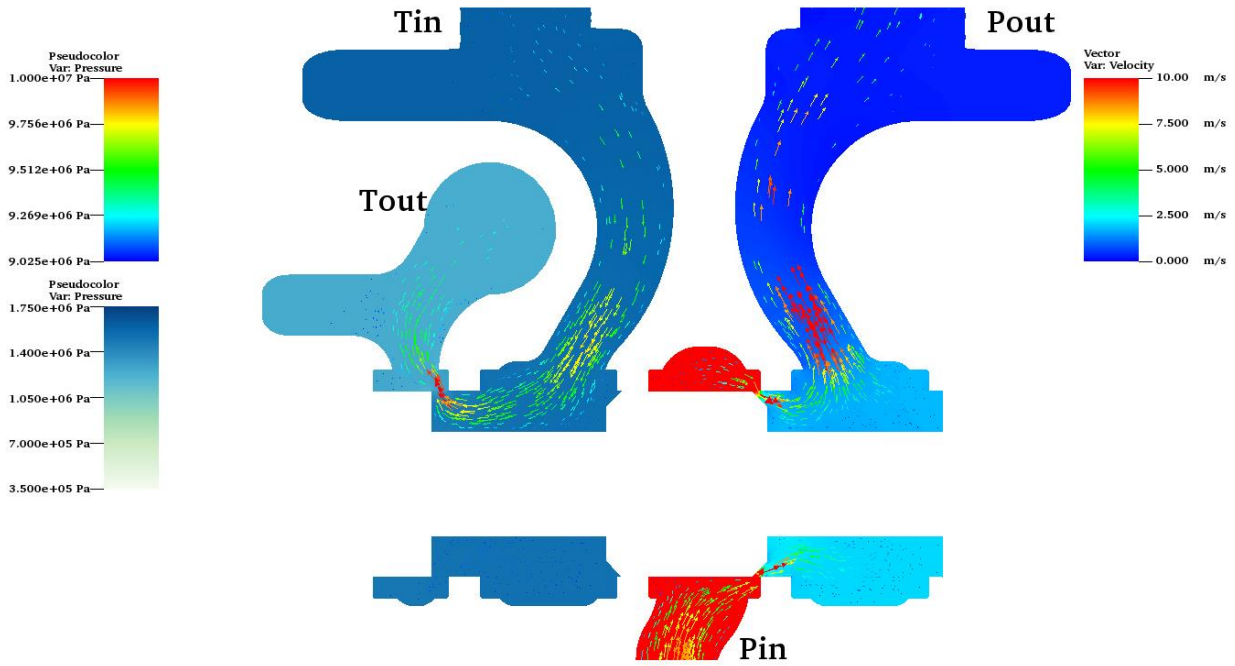
6.2.1.2 TR Half Slice Contours

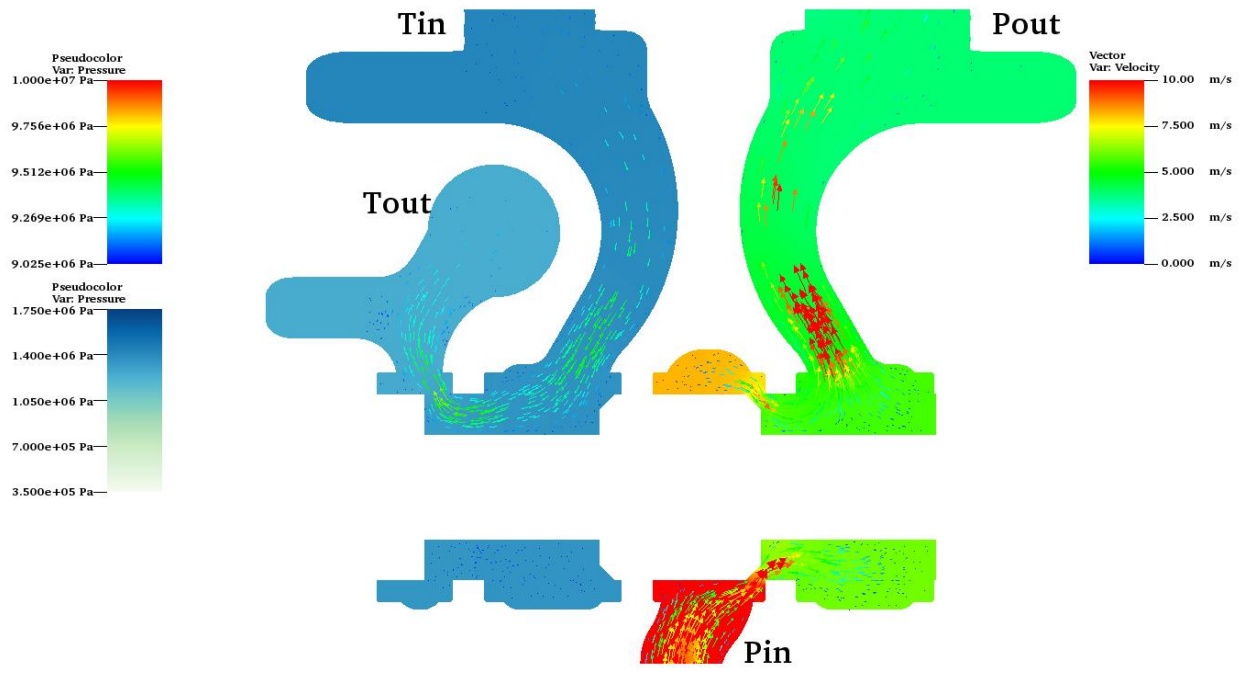*Figure 6.14: Pressure contour, velocity vectors TR 1.694mm stroke half slice*

Figure 6.15: Pressure contour, velocity vectors TR 2.804mm stroke half slice
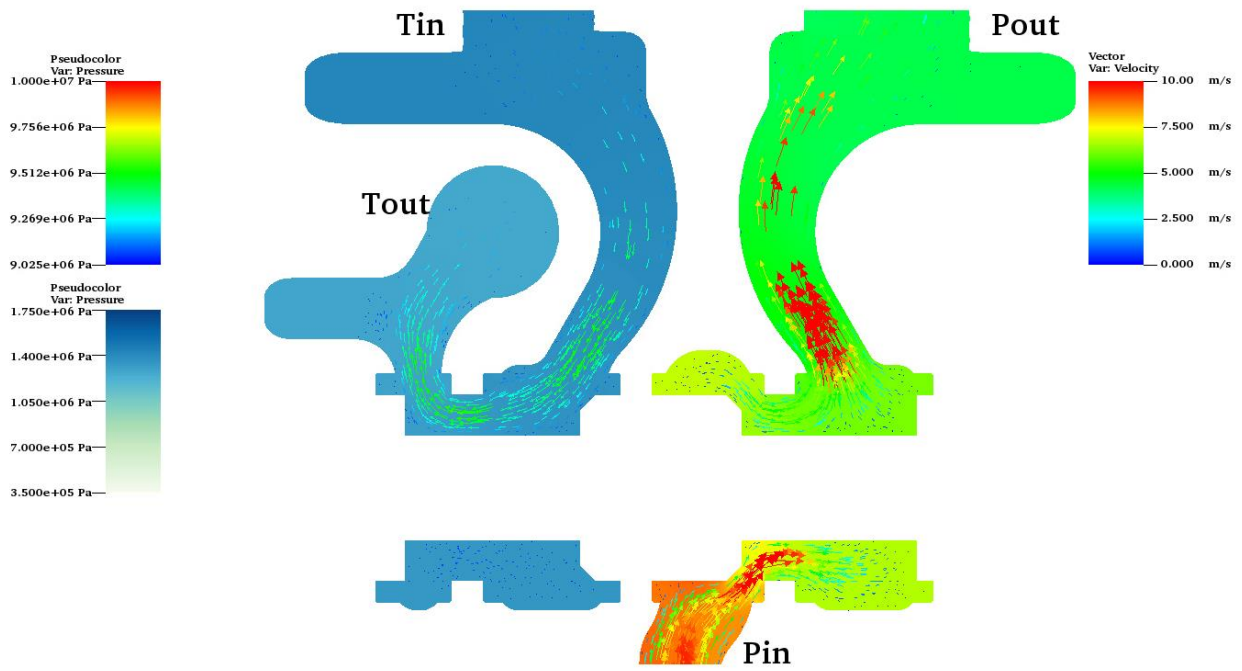

Figure 6.16: Pressure contour, velocity vectors TR 4.54mm stroke half slice
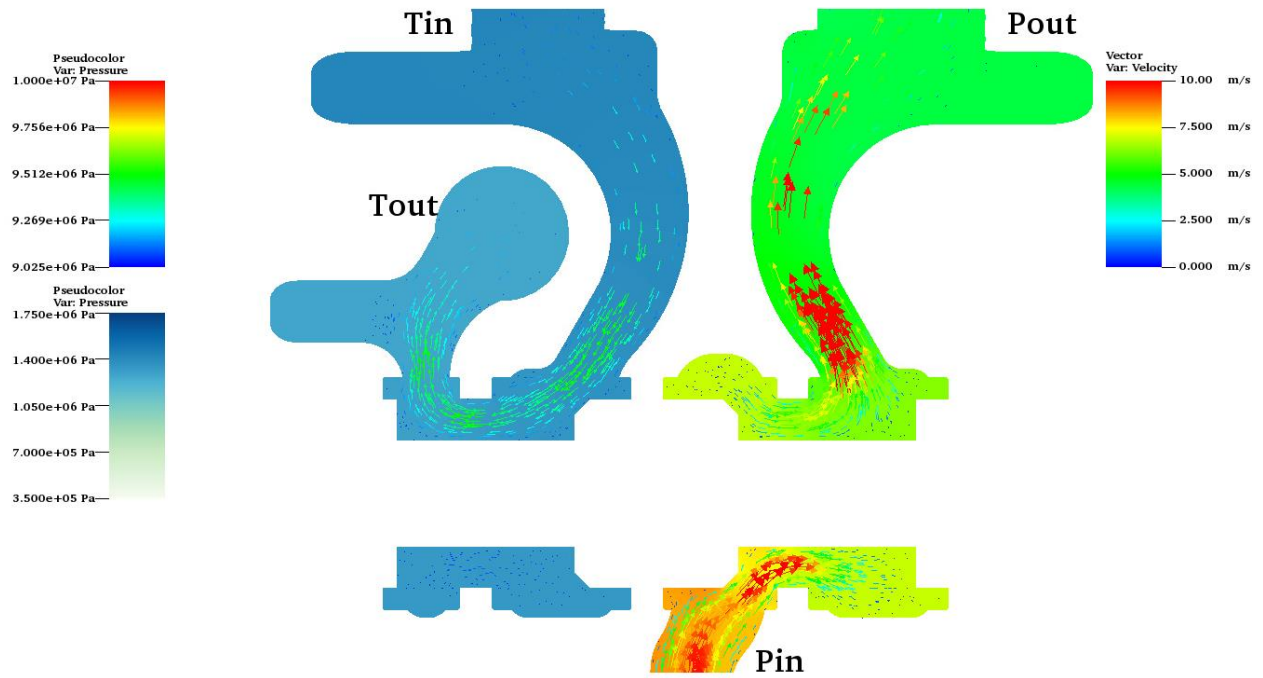
Figure 6.17: Pressure contour, velocity vectors TR 6.134mm stroke half slice
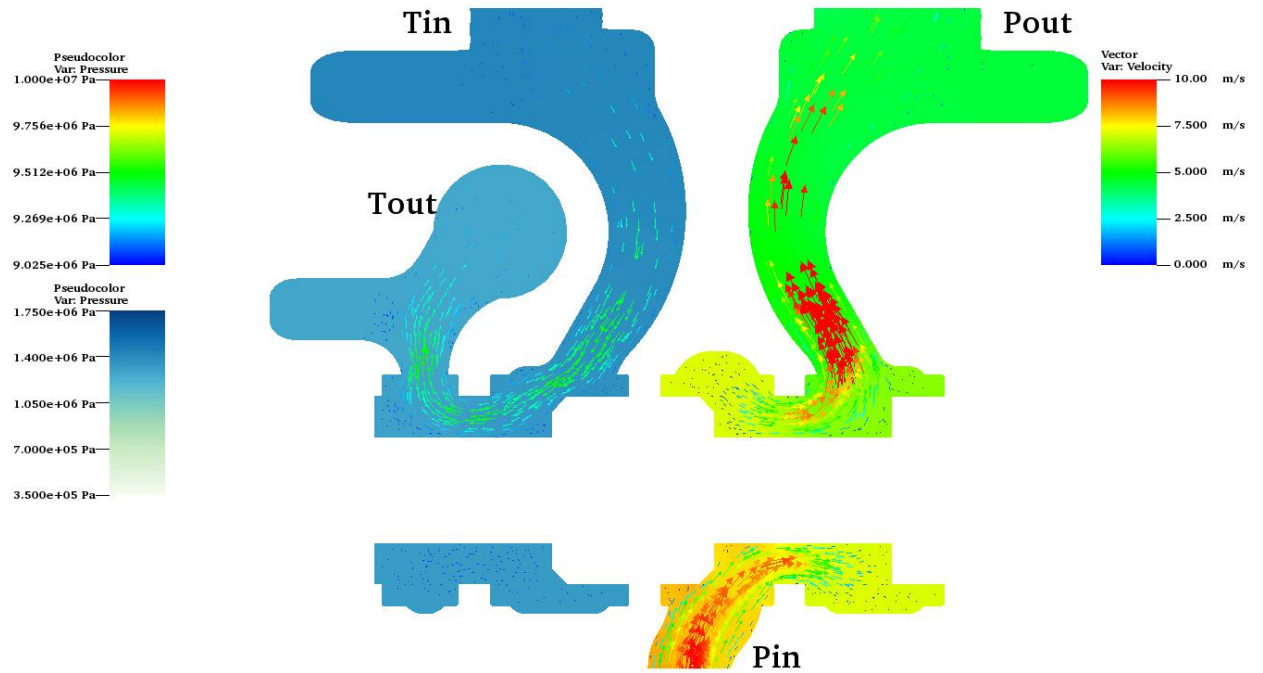

Figure 6.18: Pressure contour, velocity vectors TR 7.87 mm stroke half slice

6.2.1.3   SS Spool Slice Contours

The figures below show SS spool slice contours across the valve. The velocity vectors normal to the bottom of the valve indicate the production of turbulence as the flow attempts to move around the spool.
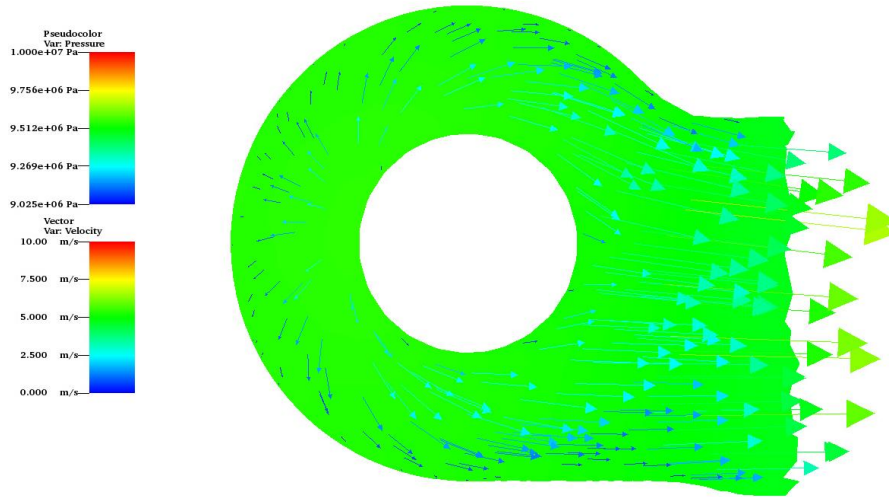

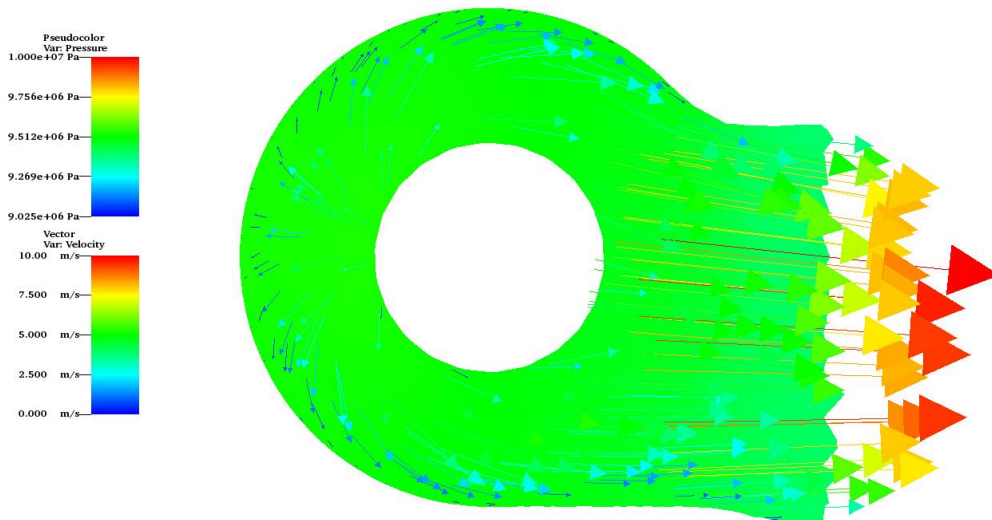*Figure 6.19:Pressure contour, velocity vectors, SS 1.54mm stroke spool*

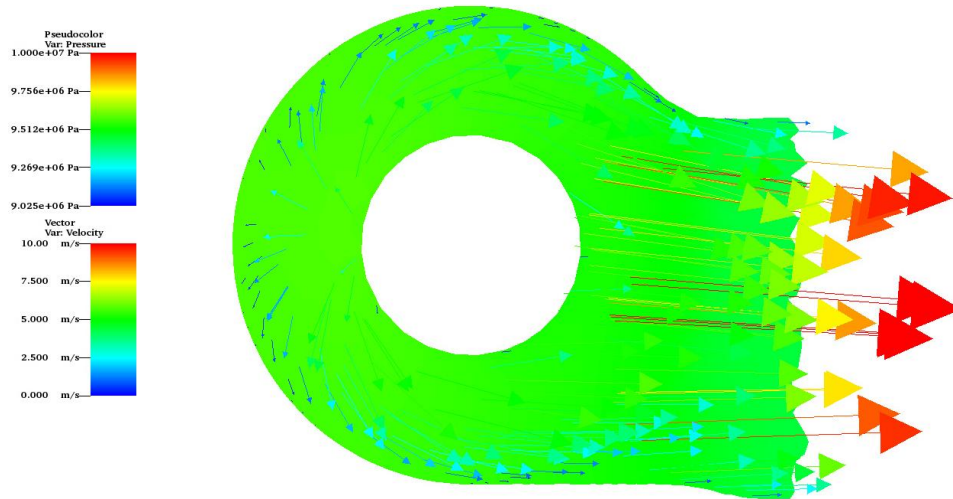*Figure 6.20: Pressure contour, velocity vectors, SS 2.88mm stroke spool*

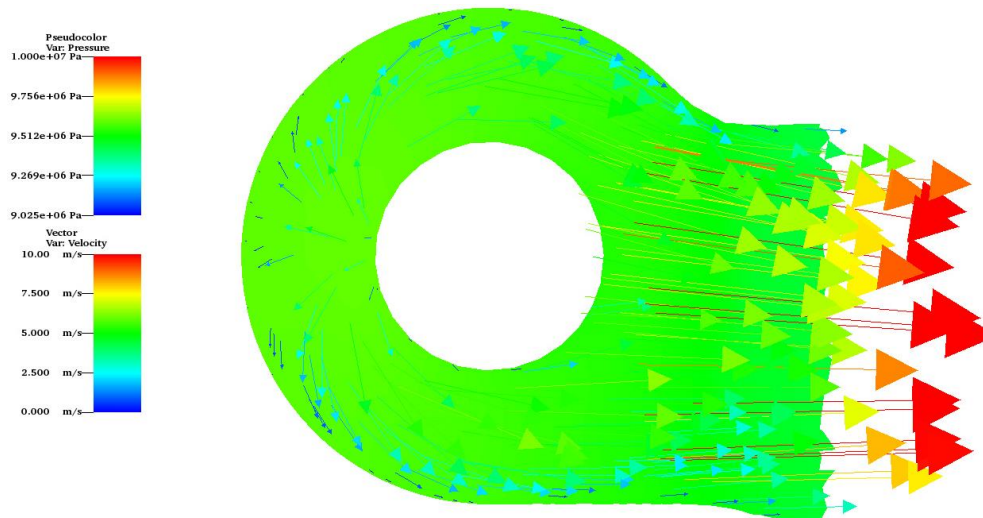*Figure 6.21: Pressure contour, velocity vectors, SS 4.54mm stroke spool*

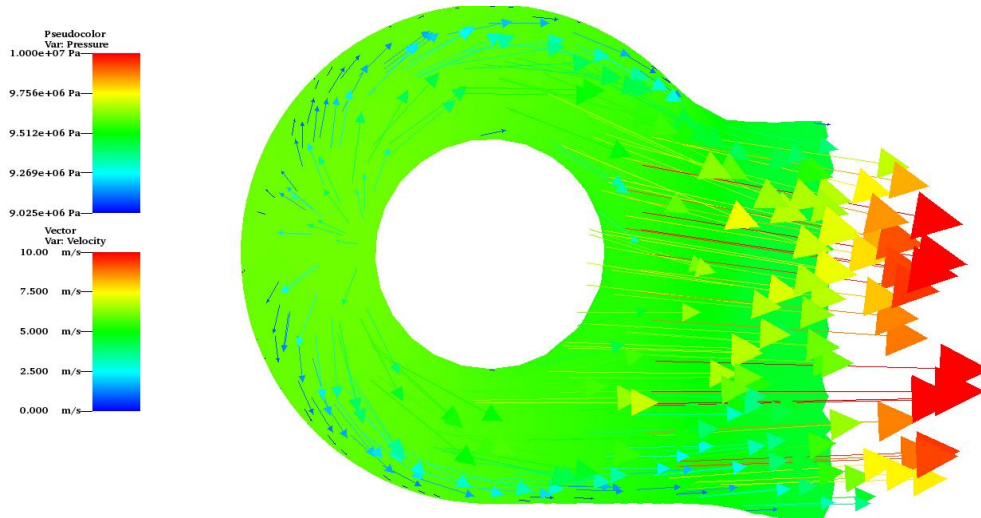*Figure 6.22: Pressure contour, velocity vectors, SS 6.21mm stroke spool*

Figure 6.23 Pressure contour, velocity vectors, SS 7.87mm stroke spool

6.2.1.4   TR Spool Slice Contours

The images below show TR spool slice contours across the valve. The *velocity* contours normal

to the bottom of the valve indicate the production of turbulence where the flow attempts to move

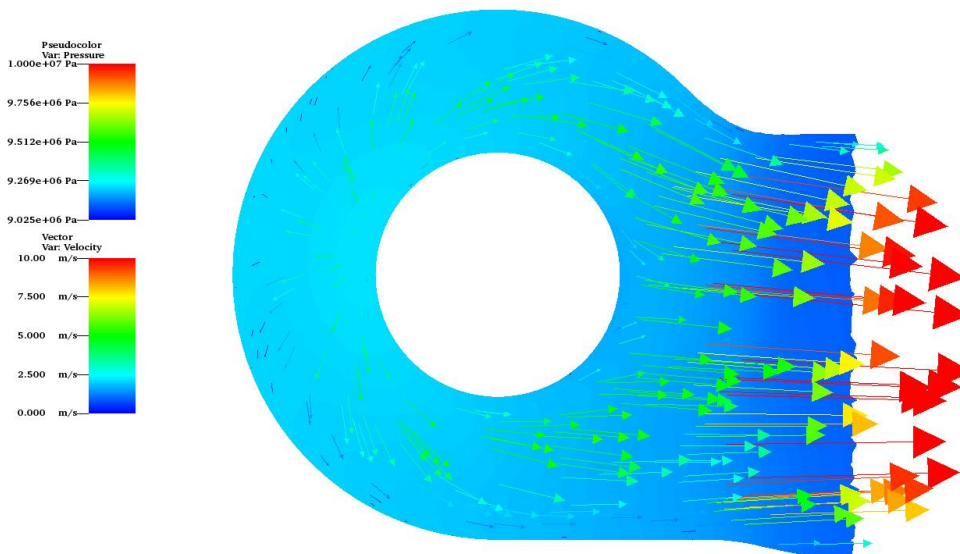around the spool.

Figure 6.24: Pressure contour, velocity vectors, TR 1.694mm stroke spool
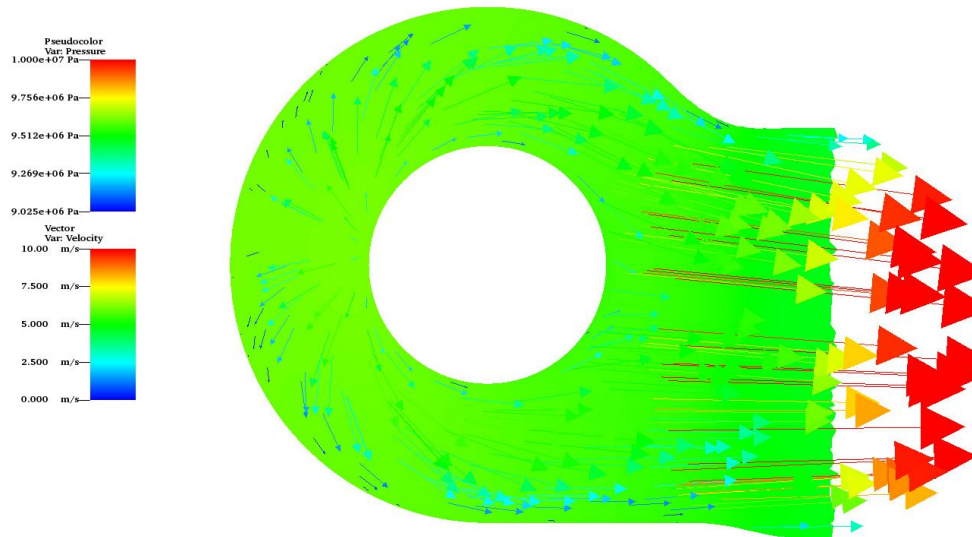
Figure 6.25: Pressure contour, velocity vectors, TR 2.804mm stroke spool
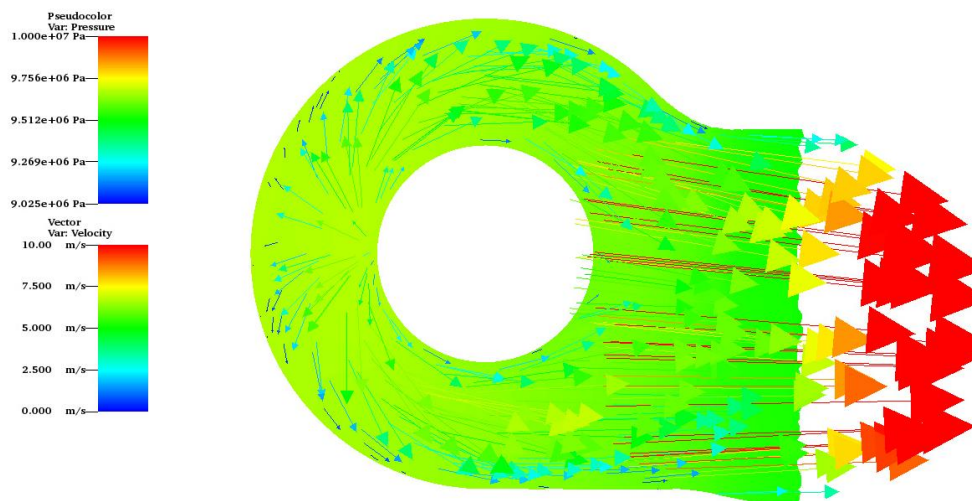
Figure 6.26: Pressure contour, velocity vectors, TR 4.54mm stroke spool
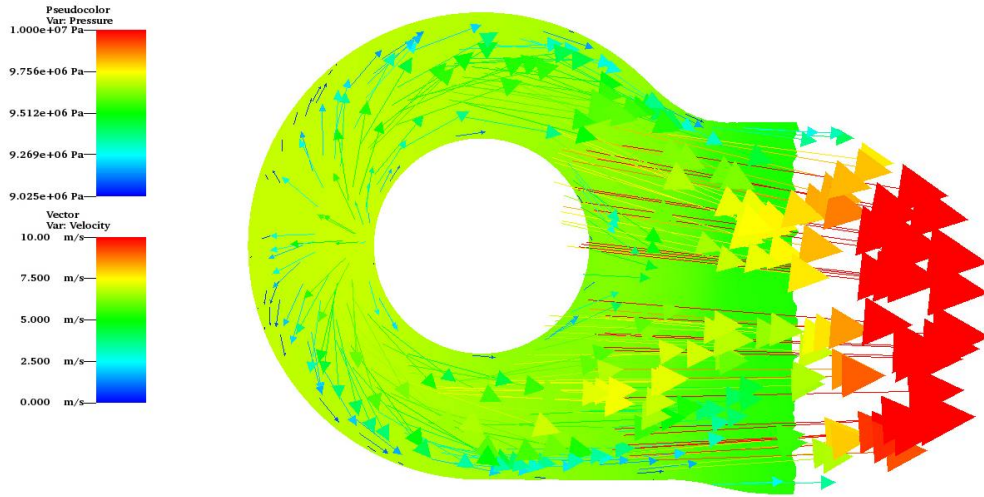
Figure 6.27: Pressure contour, velocity vectors, TR 6.134mm stroke spool
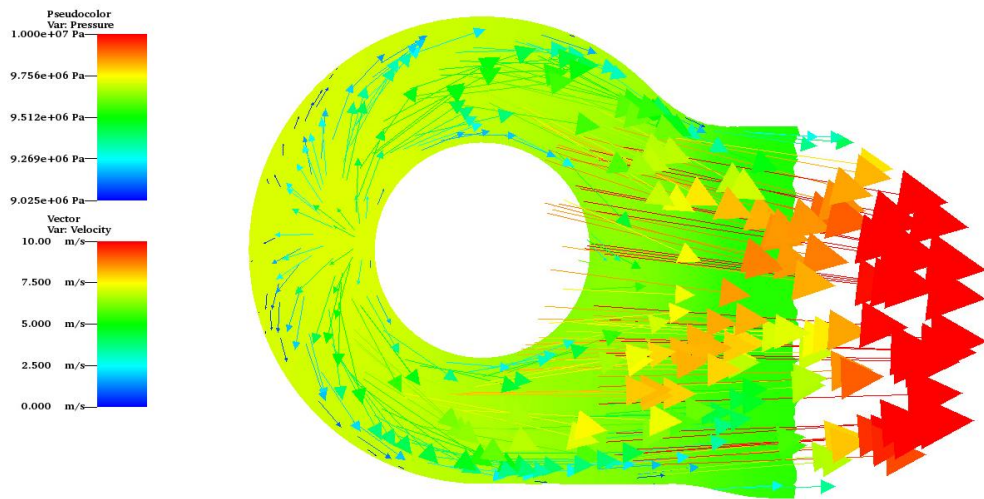
Figure 6.28: Pressure contour, velocity vectors, TR 7.87 mm stroke spool

6.2.2 Vorticity Contours

This section includes logarithmic *vorticity* contours. *Vorticity* magnitude is representative of a spinning or rotating vector and can be an indicator of secondary flows within a valve. Secondary flows can be found in both simulations in comparable locations.

6.2.2.1   SS Vorticity Contours

Figure 6.29: Log vorticity contour, velocity vectors, SS 1.54mm stroke half slice

Figure 6.30: Log vorticity contour, velocity vectors, SS 2.88mm stroke half slice

Figure 6.31: Log vorticity contour, velocity vectors, SS 4.54mm stroke half slice

Figure 6.32: Log vorticity contour, velocity vectors, SS 6.24mm stroke half slice
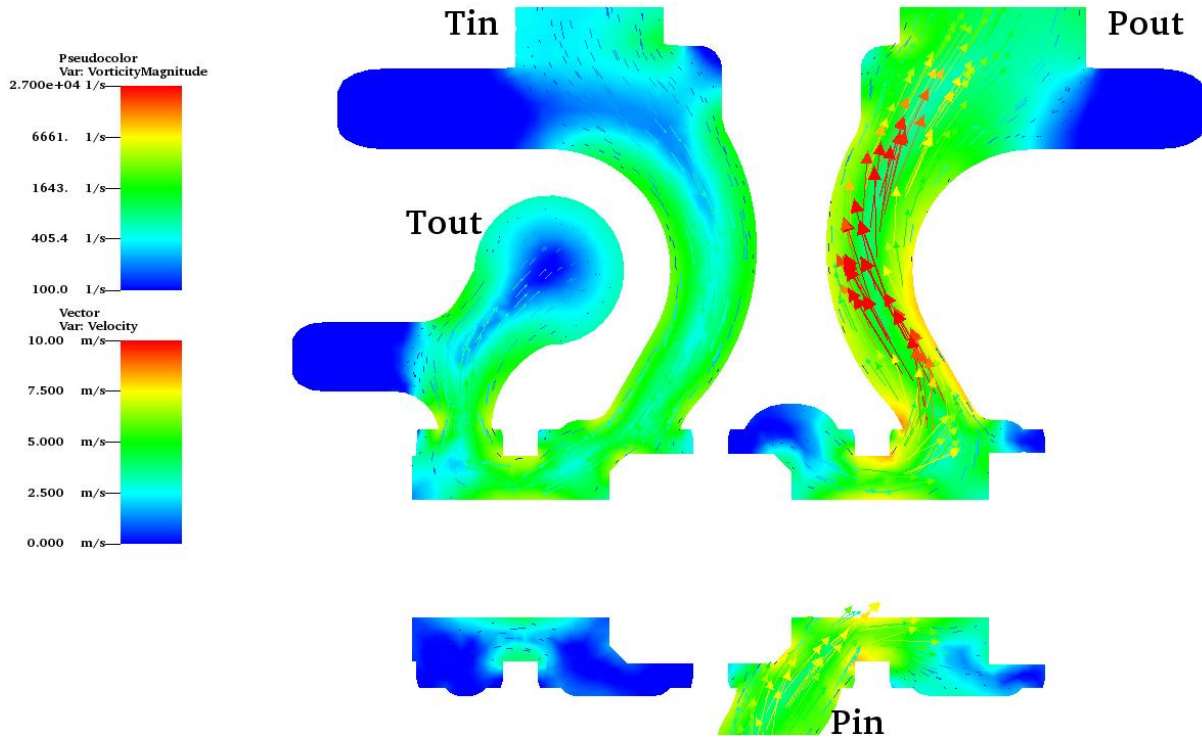
Figure 6.33: Log vorticity contour, velocity vectors, SS 7.87mm stroke half slice

6.2.2.1 TR Vorticity Contours
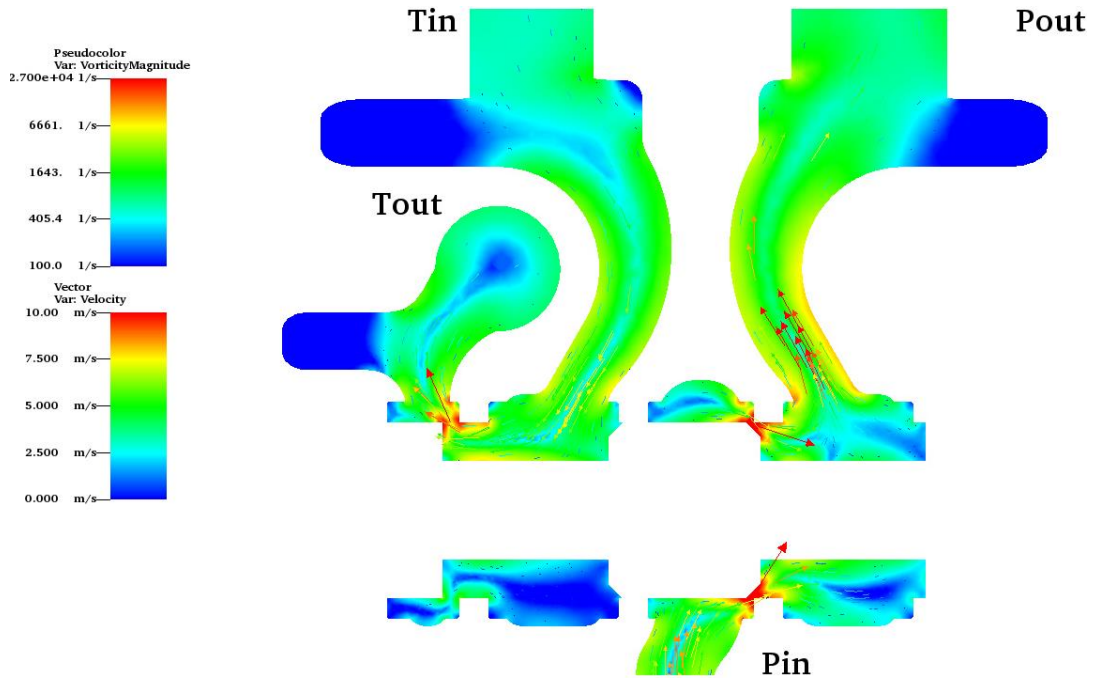
Figure 6.34: Log vorticity contour, velocity vectors, TR 1.694mm stroke half slice
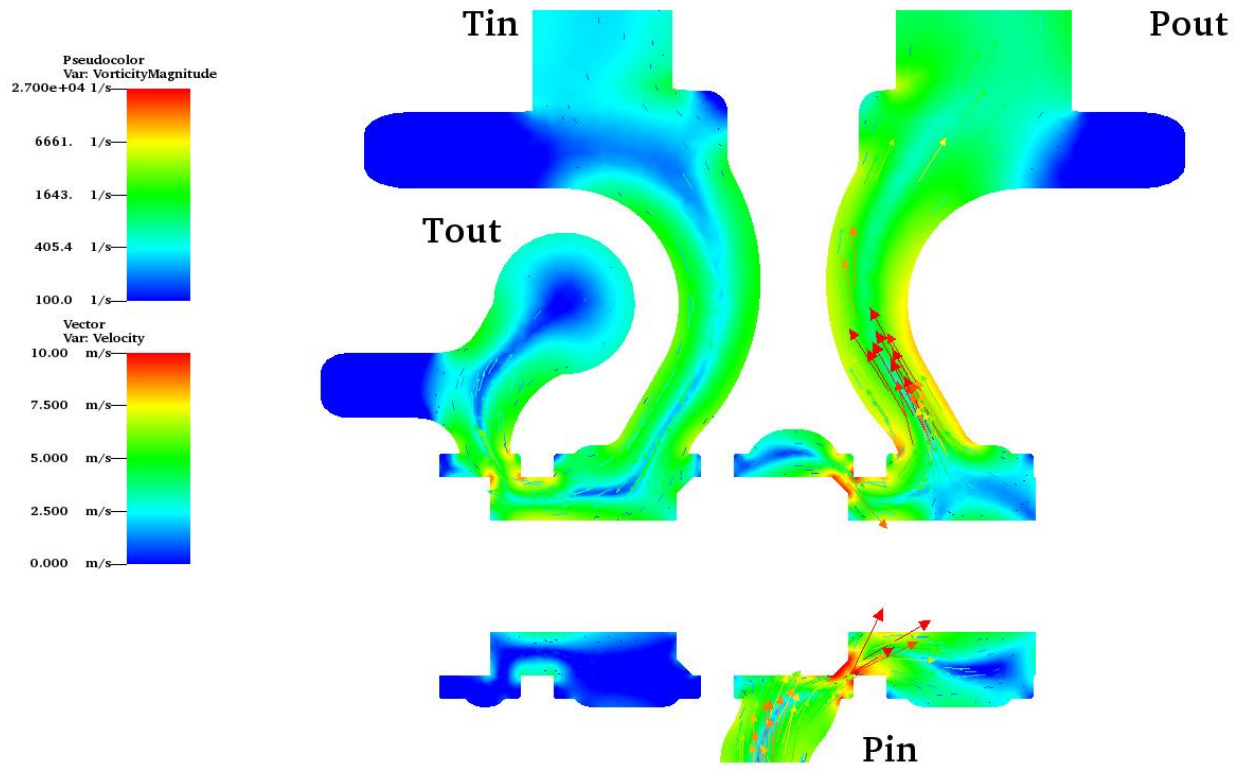
Figure 6.35: Log vorticity contour, velocity vectors, TR 2.804mm stroke half slice
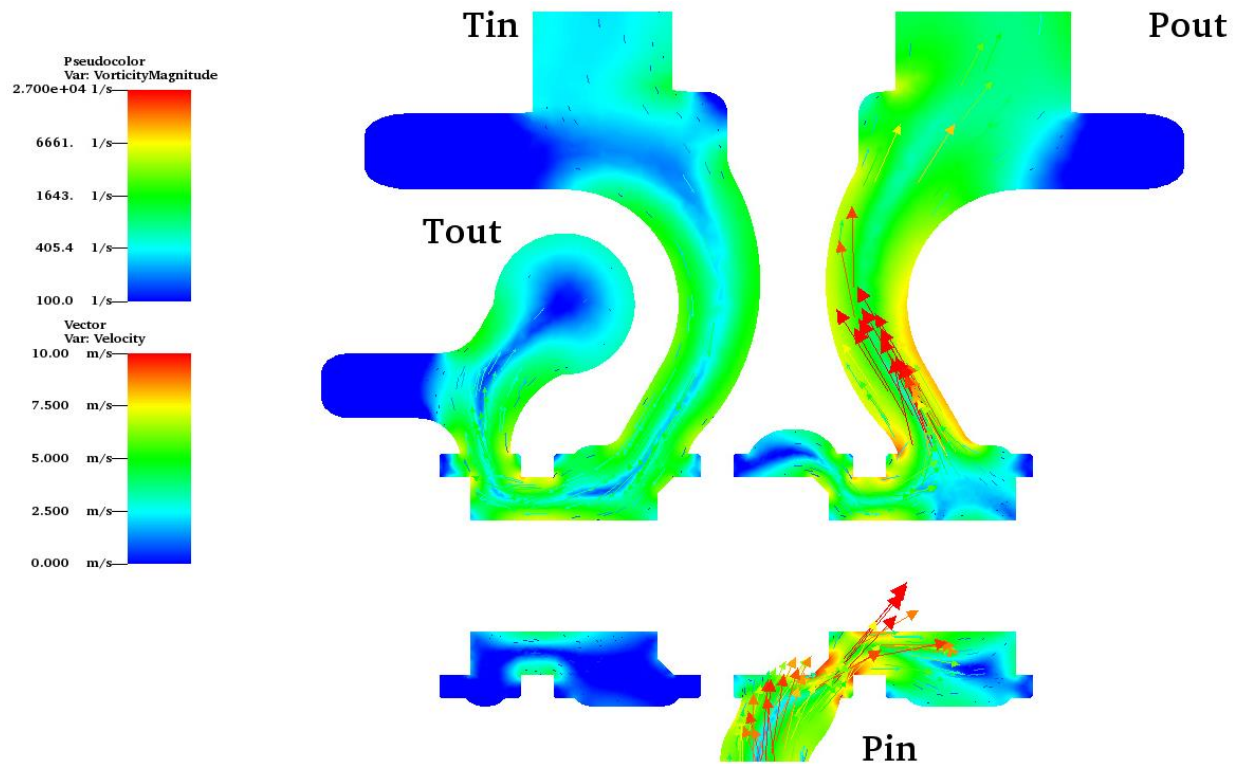
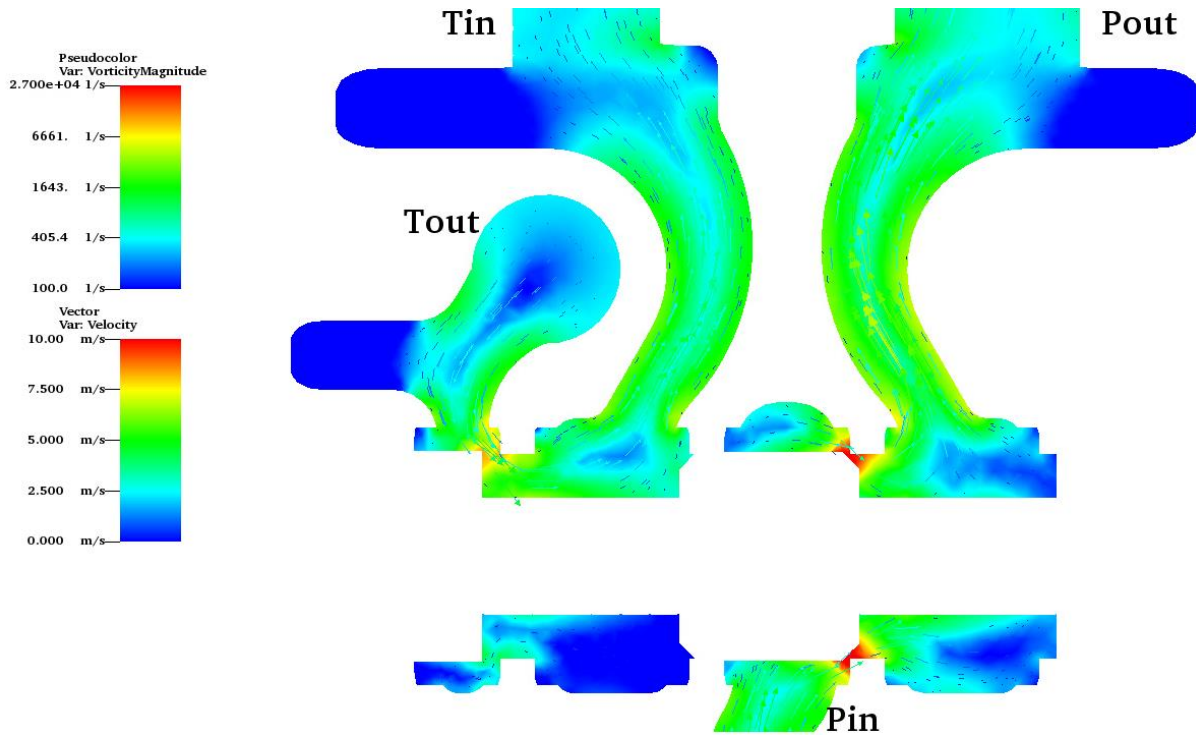*Figure 6.36: Log vorticity contour, velocity vectors, TR 4.54mm stroke half slice*

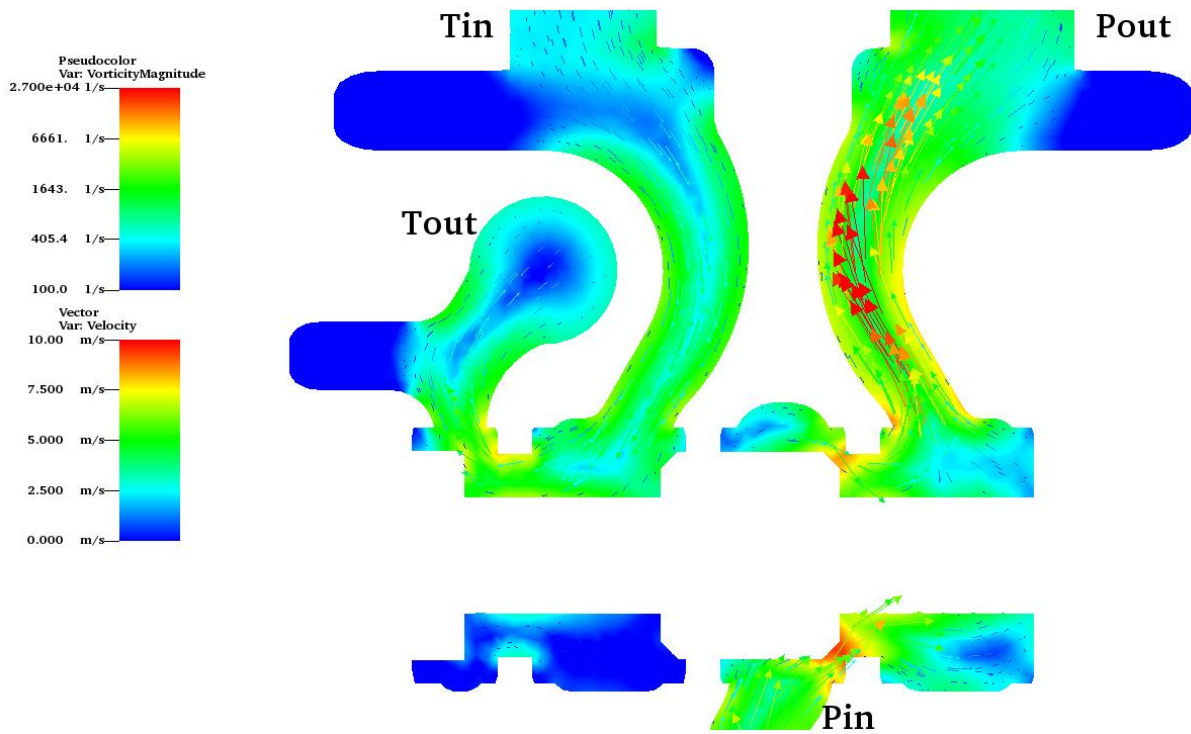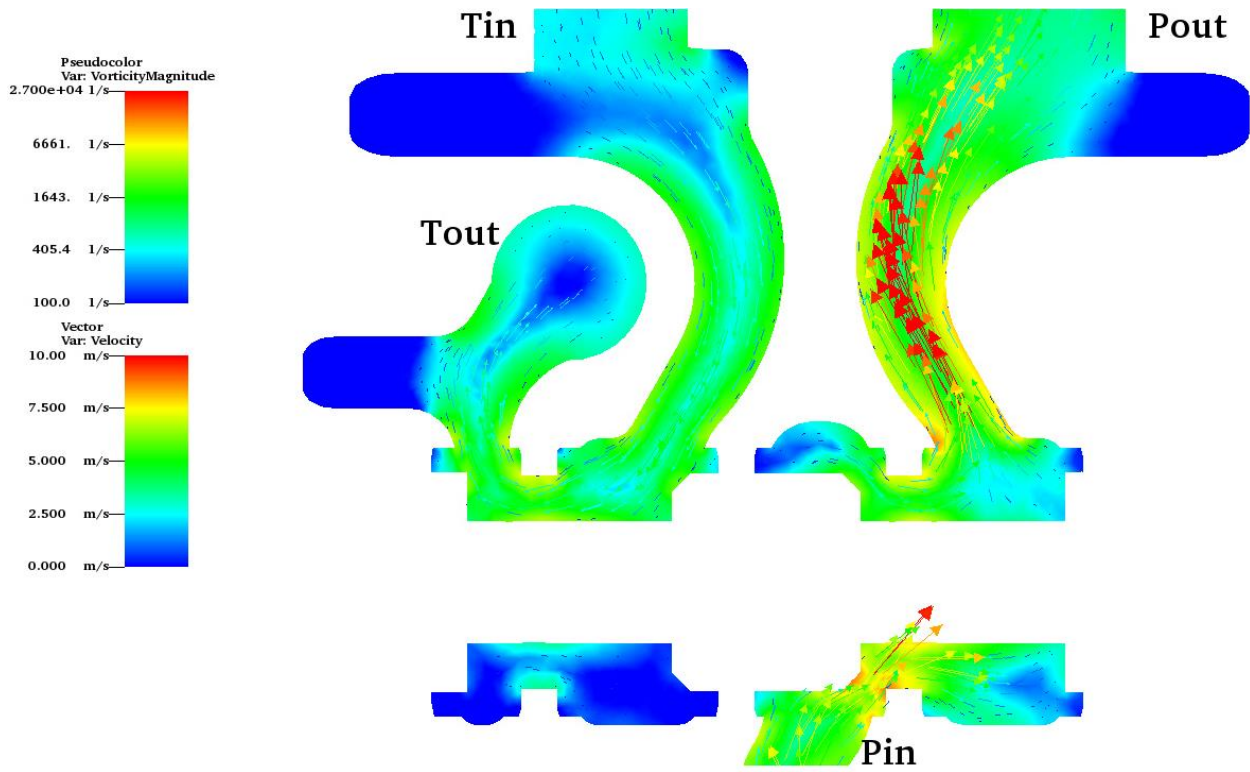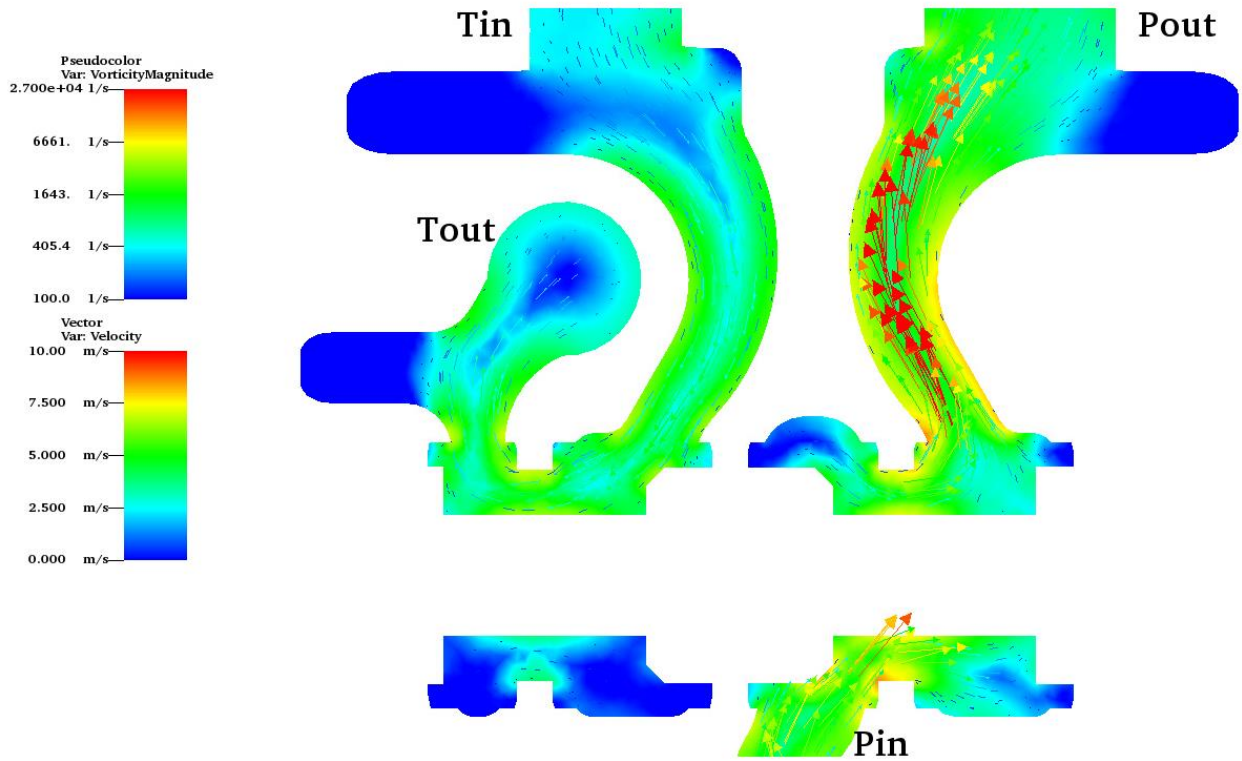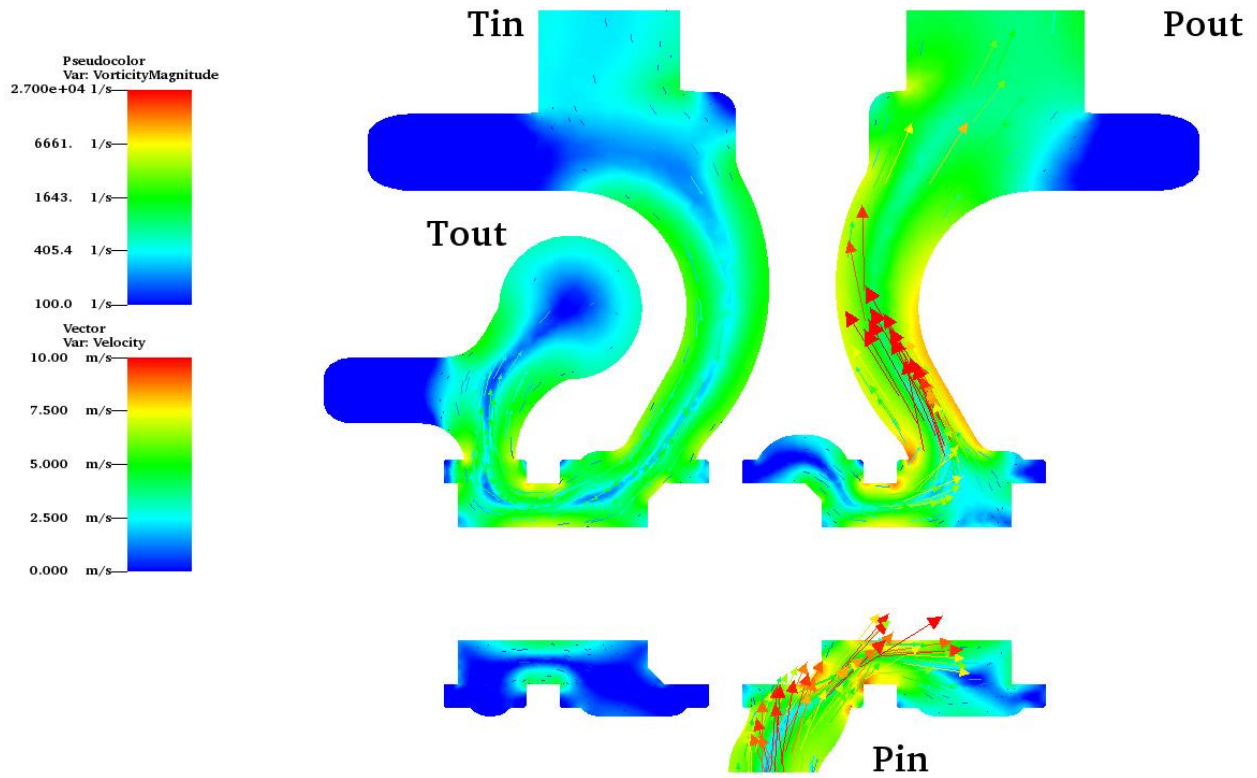*Figure 6.37: Log vorticity contour, velocity vectors, TR 6.134mm stroke half slice*
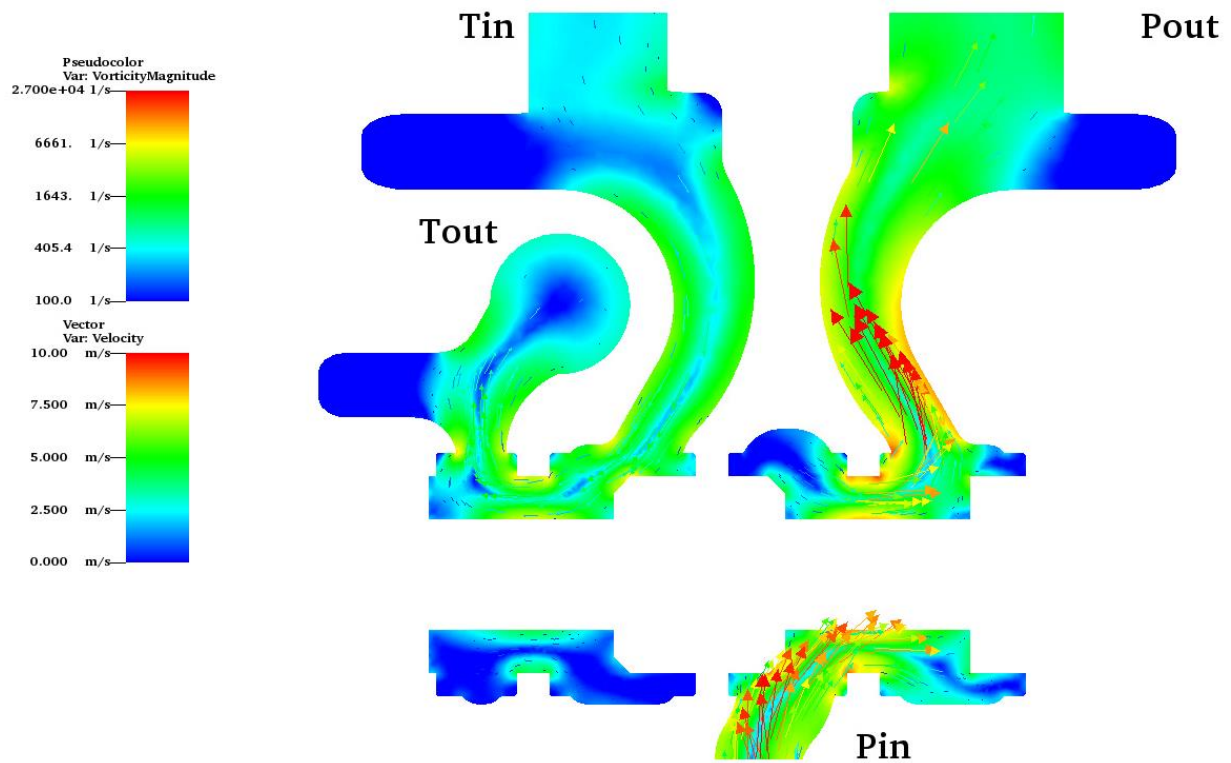
Figure 6.38: Log vorticity contour, velocity vectors, TR 7.87mm stroke half slice

Chapter 7 Discussion

7.1 Accuracy

The accuracy of the model has been calculated using percent difference with experimental flow values and has been plotted below.
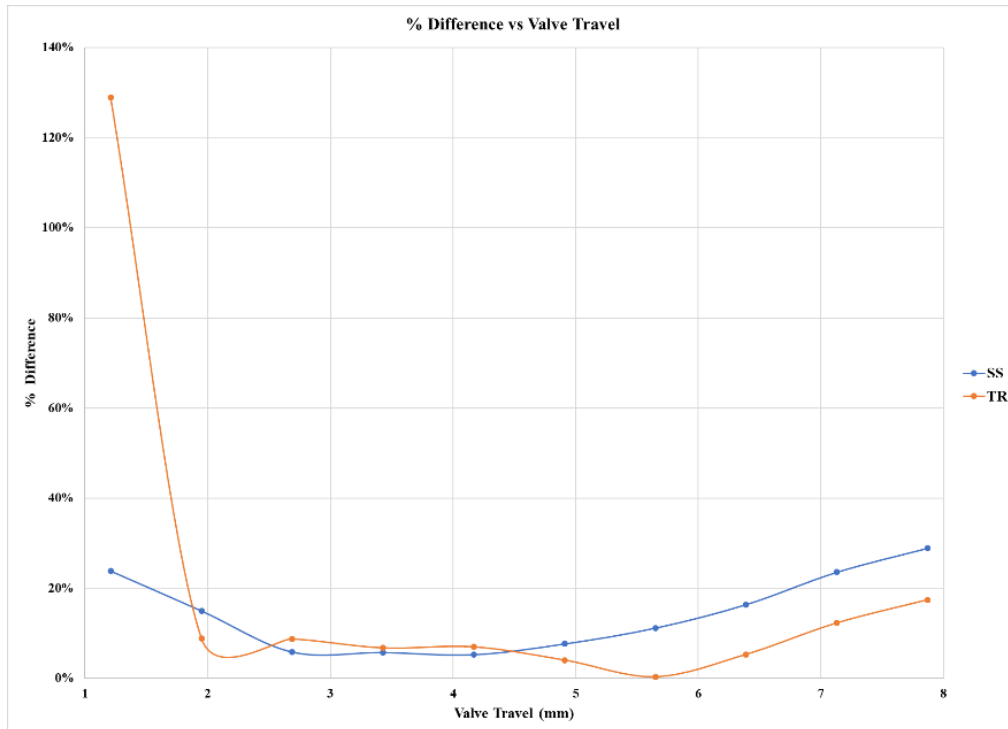
Figure 7.1: Accuracy Values

The SS simulation averaged 7.96% difference from the experimental values over the range of $1.95mm \geq X_L \geq 4.17mm$, while the TR simulation averaged 7.81% difference.

The TR simulation averaged 7.86% difference from the experimental values over the range of $4.17\ mm \geq X_L \geq 7.87\ mm$, while the SS simulation averaged 17.52% accuracy over that same range.

Both simulations had poor accuracy at low stroke values, with the SS model performing

significantly better. At valve opening the TR simulation percent difference is 129%, while the SS

had 24%.

The physical system seems to have an unexpected transient changing as the valve fully opens

however the simulations model the rise in flowrate very well until approximately 4.95*mm.*

7.2 Comparison Between Steady State and Transient Models

The percent difference between the SS and TR models was calculated by taking a percent

difference between the outputs of the simulation and evaluating the flow field parameters at

similar times across valve stroke.
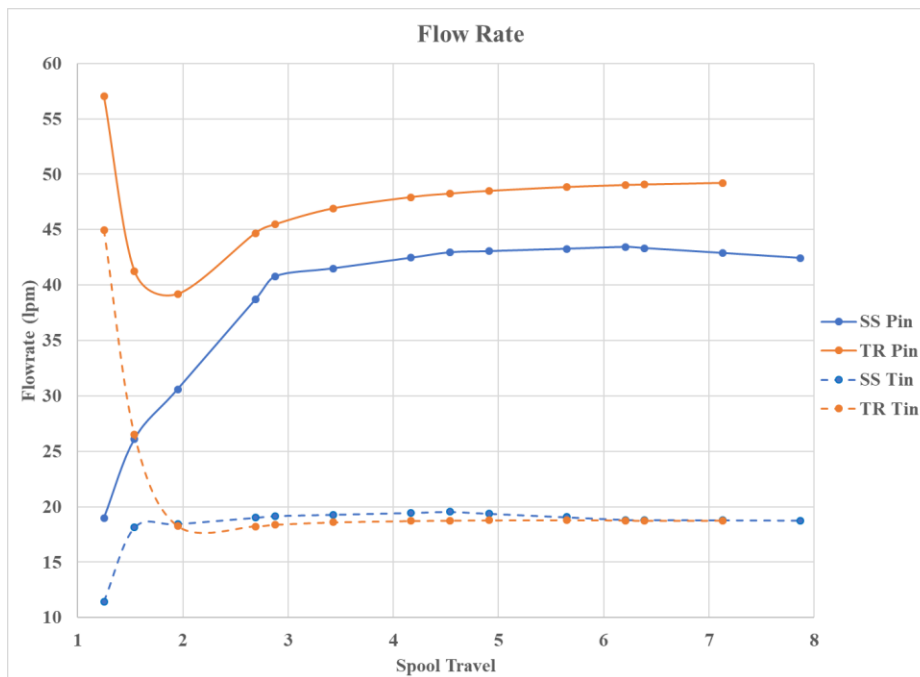
Figure 7.2: Simulation flow rates

The difference between the simulations is related to *flow rate*, which is due to the additional

convection terms present in the momentum and turbulence equations. The plot below shows the

percent difference over various spool positions. After approximately 2mm spool travel the lower

flow path through the tank portion of the valve has an average 2.5% difference with the TR

solution. At the same spool position the high flow path through the pressure portion of the valve

has an average 12.6% difference.
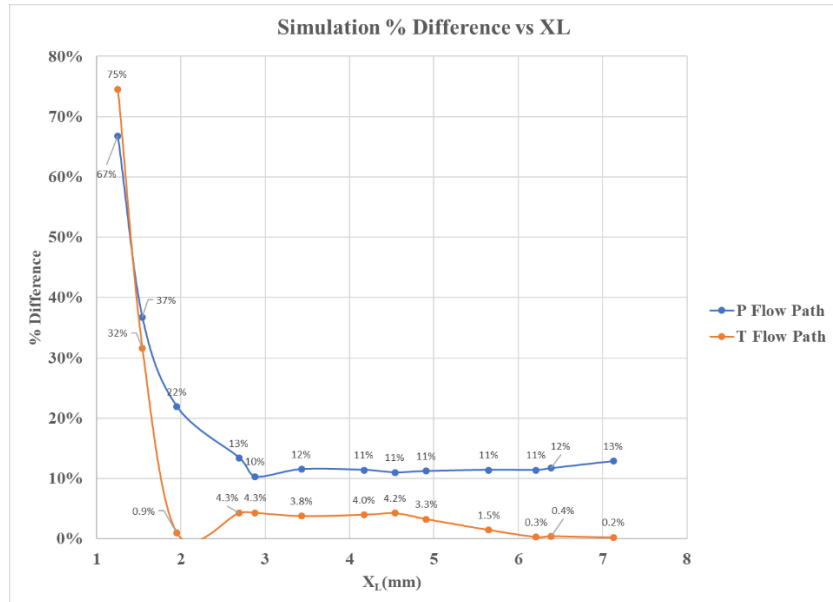
Figure 7.3: Simulation percent difference

Additionally, computation time for each simulation to run was recorded and plotted in the figure

below using a quantity of core hours. For example, a simulation that uses 40 cores and takes one

hour to run, that run consumed 40 core hours of compute time. The combined time for the SS

simulations is only approximately 31.2% the total time to run a single TR solution. Performing a

mesh refinement without a cluster would be prohibitive.
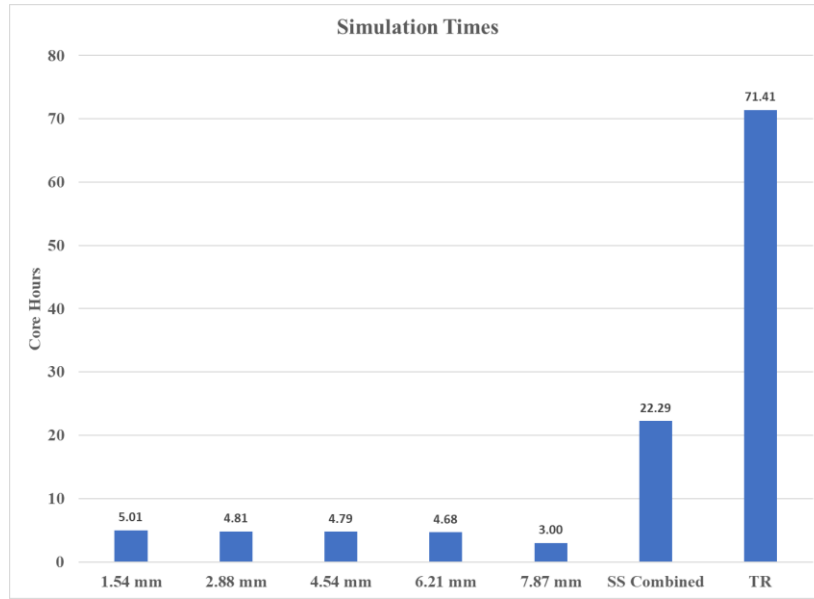
Figure 7.4: Simulation times

Chapter 8 Conclusion and Future Research

Outcomes from successfully modeling both a TR and SS simulation for the same valve geometry. Outcomes from this objective include:

- SS mesh refinement values with a total of 25 SS simulations.

- TR mesh refinement values with a total of 5 TR simulations.

- TR model development. The process to set up a TR simulation and dynamic mesh is described in Appendix B.

- SS and TR mesh refinement studies for a range of spool positions.

- Small gap geometries do not have a sufficient number of elements across the valve opening.

This study also performed a critical analysis between the SS and TR simulations. Outcomes and findings from this objective include:

- Percent difference between the SS and TR simulations at different flowrates and spool positions.

- Flow characteristics utilizing flow parameter contours.

- Pressure drop across the EHSV at two different flow rates and flow paths.

- Comparison of total computation time in core hours.

- Develop a process to evaluate two different models.

- TR model has difficulty meshing at small valve opening geometries.

Outcomes and findings from performing a critical analysis between simulation and experimental values include:

- Percent difference calculations for each point along valve stroke.

- Simulation values are an accurate representation of a real system.

- Further validates TR model has error at smaller valve opening geometries.

Further research needs to be done to fully vet out a process for industry engineers to utilize the tools developed here. Future studies could include:

- Transient boundary conditions at inlet and outlet.

- Changing viscosity and temperature and its effect on flow through the EHSV.

- Full test bench setup to validate simulation results here.

- Exploration into other transient effects in a system.

- Correlation of other turbulence models, such as k-ω turbulence model.

References

[1]   Rydberg, K.-E. (2016). Hydraulic Servo Systems : Dynamic Properties and Control.
        Linköping. Retrieved from http://urn.kb.se/resolve?urn=urn:nbn:se:liu:diva-132396

[2]   Maskrey, R. H., & Thayer, W. J. (1978). A brief history of electrohydraulic servomechanisms.
        Moog Technical Bulletin, 141.

[3]   Eriksson, Elin. (2016). CFD study of a pump trip in a pump-check valve system. Umea
        University

[4]   Zhang, Z., Jia, L., & Yang, L. (2019). Numerical simulation study on the opening process of
        the atmospheric relief valve. Nuclear Engineering and Design, 351, 106-115.

[5]   Yang, X., Keum, S., and Kuo, T. (March 1, 2016). "Effect of Valve Opening/Closing Setup on
        Computational Fluid Dynamics Prediction of Engine Flows." ASME. J. Eng. Gas Turbines
        Power. August 2016; 138(8): 081503. https://doi.org/10.1115/1.4032342

[6]   Ansys® Academic Research Fluent, Release 12.1, Help System, User Guide, ANSYS, Inc.

[7]   Diego, Bolster. Fluid Mechanics: Pipe Flow, 2006

[8]   S. Cao, S. Ozono, K. Hirano, Y. TamuraVortex shedding and aerodynamic forces on a
        circular cylinder in linear shear flow at subcritical Reynolds number J. Fluids Struct., 23
        (2007), pp. 703-714

[9]   Kuron, M. (2015, January 06). 3 Criteria for Assessing CFD Convergence. Retrieved June 26,
        2020,
        https://www.engineering.com/DesignSoftware/DesignSoftwareArticles/ArticleID/9299/3-
        Criteria -for-Assessing-CFD-Convergence.aspx

[10]   Jiyuan Tu, Guan-Heng Yeoh, & Chaoqun Liu. (2013). Chapter 3 - Governing Equations for
        CFD—Fundamentals. In Computational Fluid Dynamics (Second ed., pp. 61-121). Elsevier.

[11]   Rigola, J., D. Aljure, O. Lehmkuh, C. Perez-Segarra, and A. Oliva. "Numerical Analysis of the
        Turbulent Fluid Flow through Valves. Geometrical Aspects Influence at Different
        Positions." IOP Conference Series: Materials Science and Engineering 90.1 (2015):
        012026/1-012026/10. Web.

[12]   Pan, Xudong, Guanglin Wang, and Zesheng Lu. "Flow Field Simulation and a Flow Model of
        Servo-valve Spool Valve Orifice." Energy Conversion and Management 52.10 (2011): 3249-
        256. Web.

[13]   Huang Hao, and Lei Huihu. "Modeling and Simulation of Flow Field of Main Spool in Servo
        Valve." *Proceedings of 2011 International Conference on Electronic & Mechanical
        Engineering and Information Technology* 2 (2011): 867-70. Web.

[14]   Lisowski, Edward, and Grzegorz Filo. "CFD Analysis of the Characteristics of a Proportional Flow Control Valve with an Innovative Opening Shape." *Energy Conversion And Management* 123 (2016): 15-28. Web.

[15]   Boqvist, E. (2014). Investigation of a swing check valve using CFD.

[16]   Durst, Ray. The Development Lengths of Laminar Pipe and Channel Journal of Fluids Engineering, November 2019

[17]   Duz, H. Numerical and Experimental Study to Predict the Entrance Length in Pipe Flows; Journal of Applied Fluid Mechanics, 2019

[18]   LLNL. (2020, May). Archive of VisIt Releases. Retrieved July 22, 2020, from https://wci.llnl.gov/simulation/computer-codes/visit/releases

[19]   White, F. M. (2016). Fluid mechanics. New York, NY: McGraw-Hill.

[20]   Erke Wang, T. N., & Rauch, R. (2004). Back to elements-tetrahedra vs. hexahedra. In Proceedings of the 2004 international ANSYS conference.

Chapter 9 Appendices

Appendix A: UDF Function

Appendix B: TR Simulation Setup

Appendix A: UDF

```
/*Servo Valve motion*/
/*UDF defining linear motion of the vale*/
/*              */

#include "udf.h"
#define v_grade -0.074
#define v_intercept 0.0012



DEFINE_CG_MOTION(valve_motion, dt, cg_vel, cg_omega, time, dtime)
{
        real velocity;

                cg_vel[0] = v_grade;
                cg_vel[1] = 0.0;
                cg_vel[2] = 0.0;

                cg_omega[0]= 0.0;
                cg_omega[1]= 0.0;
                cg_omega[2]= 0.0;
                }
```

Figure 9.1:UDF function

Appendix B: Transient Simulation Setup

The following steps detail the setup of the Transient Simulation.

1. Produce the two geometries separately. The first zone represents the stationary zone with a typical mesh. The second zone is the dynamic moving zone.

   a. Note: When creating geometry in CAD software, export step files from an assembly to ensure that they will be in the correct location in Ansys®.

2. Using Ansys® Workbench® create a separate mesh for each zone.

3. Create a *.cas file* for the dynamic meshing region using the setup window in Fluent®.

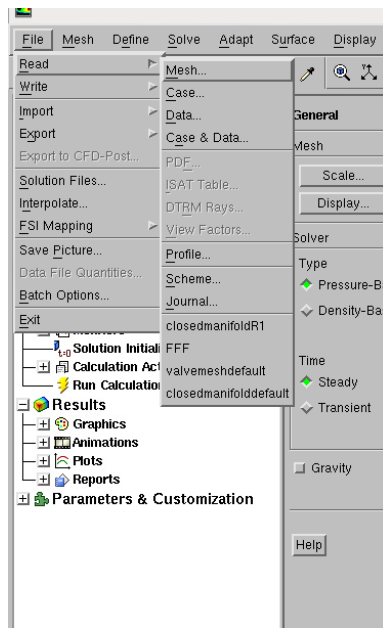4. Open a new Fluent® module and import the stationary mesh.

Figure 9.2: Mesh import interface

5. Append the dynamic mesh case file by selecting mesh→zone→append_cas_file
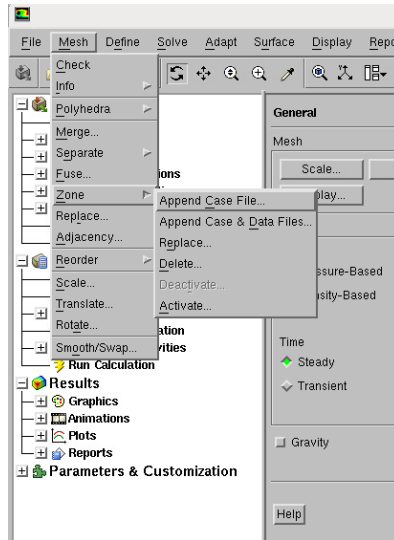
Figure 9.3: Case file append interface

6. Create the mesh interface by first deleting the interfaces created by Fluent® when the

    mesh was appended.

    a. Note: Fluent created contact regions. In order for the simulation to work correctly
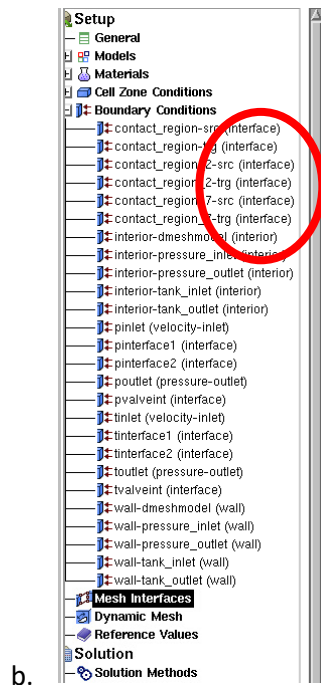
        default interfaces need to be changed to walls.

Figure 9.4: Default interface settings

60

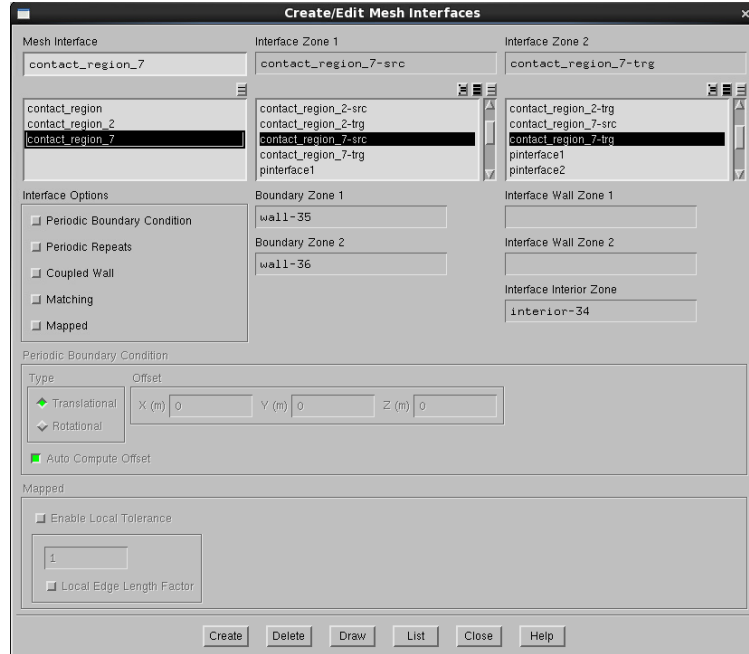c. Default interfaces are shown below, generally called "contact_region_".

Figure 9.5: Mesh interface settings

d. Once default interfaces have been deleted and surfaces changed to walls, the only

visible surfaces in this window should be the surfaces created specifically for the
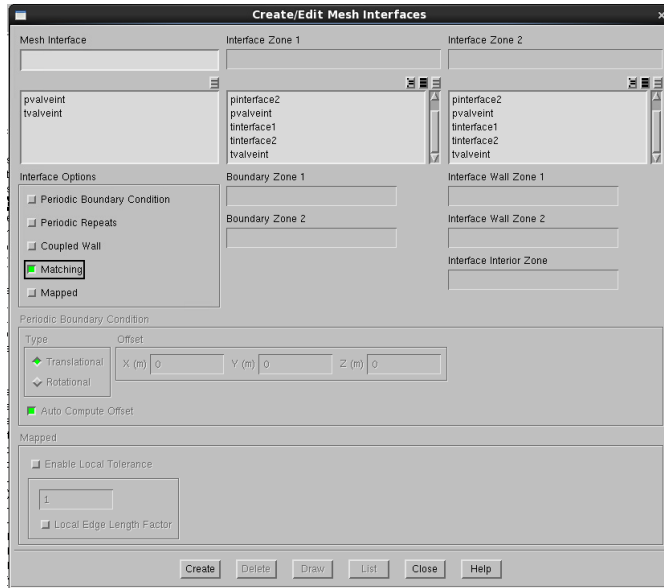
mesh interface.

Figure 9.6: Correct mesh interface settings

7. Compile the User Defined Function (UDF)

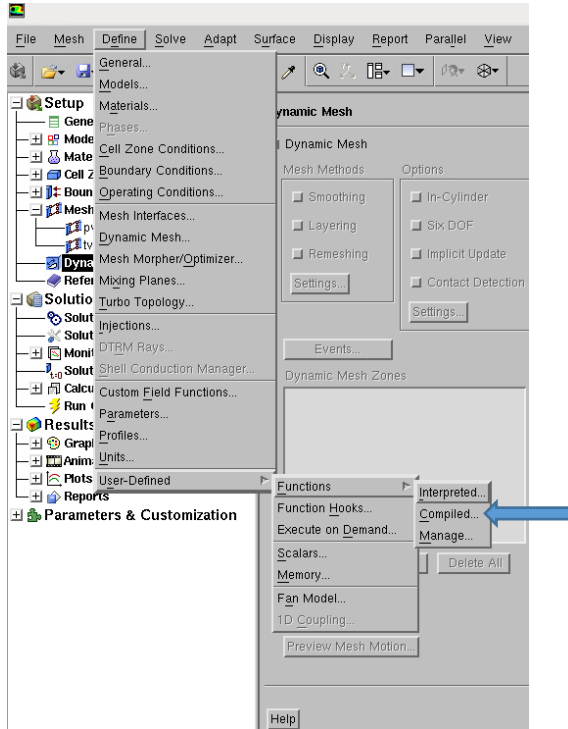 a. Select compile from the menu: Define→User-Defined→Functions→Compiled

Figure 9.7: Compiled UDF selection

b. Add the source file to the list by clicking *Add* and choosing file.

   i. Note: Source file must be saved in the same folder with both the *.cas* and *.dat files* for simulation.

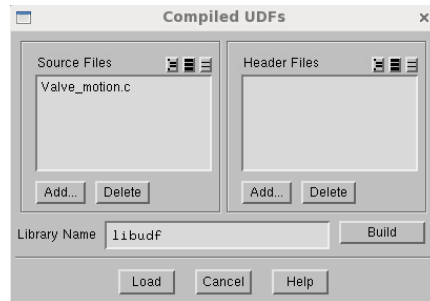c. Build the library by choosing source file and selecting *Build.*

Figure 9.8: UDF library creation

d. Load the source file by selecting the *Load* button.

   i. Note: Library must be built the library prior to loading the compiled UDF.

8. Create the dynamic mesh zone.

   a. Check the dynamic mesh box under the dynamic meshing option.

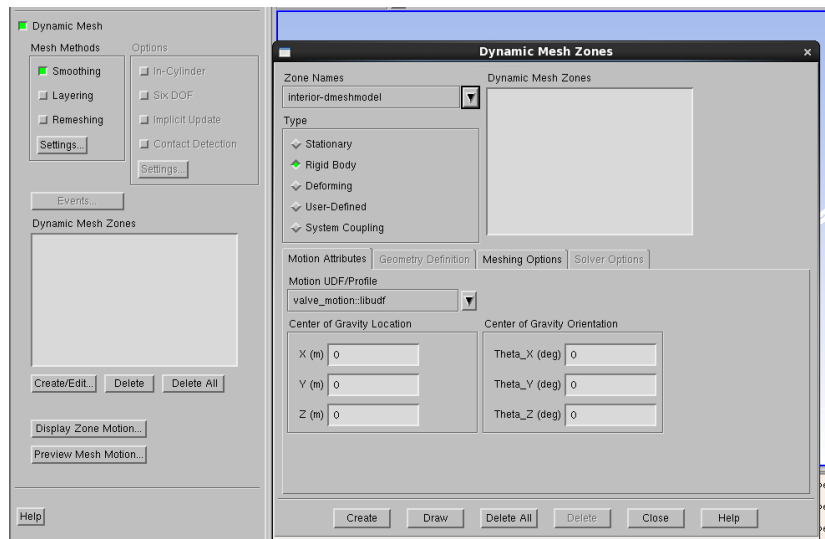   b. Assign dynamic meshing zone to interior of dynamic mesh.

Figure 9.9: Dynamic meshing zone settings

c. Verify UDF has been assigned to the motion of that zone. If UDF has not been compiled before this point, no motion profile will be available to select.

d. Create the dynamic mesh zone by selecting *Create*.

9. Create a dynamic meshing event. This will initialize the valve motion.

a. Select *Events* option in dynamic meshing menu.

b. Increase the number events to 1 using the up arrow to adjust the number.

c. Edit event 1 by selecting *Edit*.

d. For event type select *Change Motion Profile*.

e. Select *Close*

f. Choose time for motion to start changing which should be after the first time step.

10. Using these instructions, the model will have a dynamic mesh that will begin moving after the first time step.